PLAXIS

CONNECT Edition V22.00

User Defined Soil Models:

N2PC-MCT: A VISCOPLASTIC CREEP MODEL INCLUDING A PLASTIC FAILURE MECHANISMFOR ROCKS [ULT]+[GSE]

Last Updated: January 14, 2022

Table of Contents

1 Introduction

Many types of rocks (for instance claystone, sandstone, and especially rock salt), exhibit time-dependent behaviour (Bui, et al., 2017) (Gramheden & Hokmark, 2010). Creep of rocks and rock salts is related to various applications in civil engineering, mining industry or petroleum engineering, such as energy storages, wellbore stability in oil and gas extraction, radioactive waste facilities design etc (Cornet, et al., 2018). For instance, drilling a deep borehole (around 5000m of depth) for oil extraction could face a serious instability problem when going through a creeping salt layer (see Figure 1)

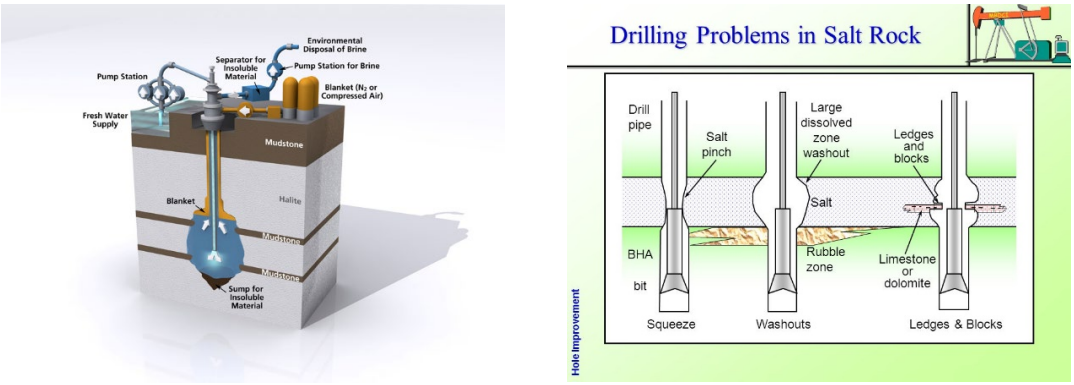

Figure 1 Rock Creep-related issues

Most of underground applications concern with large time scales (tens to thousands of years or even longer) and thermal effects at high depth (hundreds to thousands of meters depth). The Norton power creep law (Norton, 1929) is widely used for describing the steady state creep behaviour, which is relevant for those large time scales. In this context, an enriched version of the Norton law, the Norton-based Double Power Creep (N2PC) model, including temperature effects, was implemented as a PLAXIS UDSM in 2018.

The N2PC model is particularly useful for studying the time-dependent (long-term) deformation of rock structures (for example subsidence analysis for solution mining). In some situations, not only deformation but stress analysis is also important to predict failure and damage of the structures. To better capture this aspect, the model is further extended by including a Mohr-Coulomb with Tension cut-off (MCT) failure mechanism. The extended model, called N2PC-MCT model, allows modelling more adequately both instantaneous plastic deformation and stress evolution related to rock plastic strength parameters.

In the following both the original version (N2PC) and the extended version (N2PC-MCT) will be presented. Throughout this document, tensor and vector quantities are denoted in bold while scalars are in normal character. Continuum mechanics convention is used, namely tensile stresses and strains are positive. Compressive pore pressure (saturated media) is therefore negative, while suction in unsaturated materials is positive. All these conventions are consistent with the Plaxis software's.

2 Theoretical and Implementational description of the N2PC and N2PC-MCT models

2.1 Norton's creep law

The Norton's creep law (Norton, 1929) describes the creep strain as a function of the stress level as follows:

$$\dot{\boldsymbol{\varepsilon}}^{\boldsymbol{vp}} = Aq^N \frac{3\boldsymbol{s}}{2q} \tag{1}$$

where $q = \sqrt{\frac{3}{2}\boldsymbol{s}:\boldsymbol{s}}$ the Von-Mises shear stress, A and N are two model parameters.

This law is widely used in the literature, especially to describe the creep behaviour of rock salt. The parameters A and N can be easily calibrated by plotting in the logarithm scale deviatoric stress versus creep strain rate.

Note that to be consistent, the unit of A should be: *1/time unit/(stress unit)^N,* for instance, if N=3.5 then the unit of A is: 1/ *time unit* /(MPa)$^{-3.5}$

2.2 General non-isothermal framework of the N2PC model

The N2PC constitutive law is formulated based on the original Norton's law (1). The whole constitutive model is written in terms of the generalised effective stress $\boldsymbol{\sigma}'$ (accounting for both saturation degree and Biot's pore pressure coefficient) as defined in Plaxis Manuals (for instance (Plaxis, 2021) Eq 2.34). This amounts to saying that the constitutive law described below models the relationship between the strains and effective stresses.. In the following, the prime symbol is dropped for convenience and the effective stress tensor will be simply denoted $\boldsymbol{\sigma}$. This effective stress tensor can be decomposed into an isotropic part and a deviatoric part:

$$\boldsymbol{\sigma} = \sigma_m \boldsymbol{\delta} + \boldsymbol{s} \tag{2}$$

where σ_m is the mean effective stress, $\boldsymbol{s}$ the deviatoric stress tensor and $\boldsymbol{\delta}$ the second-order identity tensor.

The rock is modelled as an isotropic thermo-elasto-viscoplastic material of which the total strain tensor is decomposed as an elastic part and a viscoplastic creep part:

$$\boldsymbol{\varepsilon} = \boldsymbol{\varepsilon^e} + \boldsymbol{\varepsilon^T} + \boldsymbol{\varepsilon^{vp}} \tag{3}$$

The elastic strains obey the classic Hooke law:

$$\dot{\boldsymbol{\varepsilon}}^{\boldsymbol{e}} = \dot{\boldsymbol{e}}_{\boldsymbol{d}}^{\boldsymbol{e}} + \dot{\epsilon}_v^e \boldsymbol{\delta} \tag{4}$$

$$\dot{\epsilon}_v^e = \frac{1}{K}\dot{\sigma}_m \tag{5}$$

$$\dot{\boldsymbol{\varepsilon}}_{\boldsymbol{d}}^{\boldsymbol{e}} = \frac{1}{2G}\dot{\boldsymbol{s}} \tag{6}$$

where ϵ_v^e is the volumetric elastic strain; $\boldsymbol{e}_{\boldsymbol{d}}^{\boldsymbol{e}}$ is the deviatoric elastic strain tensor; K and G are the elastic drained bulk and shear moduli, respectively. The overdot notation denote time derivative of an *arbitrary quantity* $\dot{r} = \frac{dr}{dt}$. Remind that the bulk and shear moduli are related by:

$$K = \frac{E}{3(1-2\nu)} = \frac{2(1+\nu)}{3(1-2\nu)}G \tag{7}$$

The thermo-elastic strains (due to thermal expansion) are already taken into account in PLAXIS 2D software together with the Thermal module. They are thus not considered in the constitutive model. For completeness, thermal strain increments are recalled here:

$$\dot{\boldsymbol{\varepsilon}}^{\boldsymbol{T}} = \begin{bmatrix} \alpha_{Tx} & & \\ & \alpha_{Ty} & \\ & & \alpha_{Tz} \end{bmatrix} \dot{T} \tag{8}$$

where T denotes the temperature, and $\alpha_{Tx}, \alpha_{Ty}, \alpha_{Tz}$ are the anisotropic thermal expansion coefficients.

The viscoplastic strains are modelled as follows:

$$\dot{\boldsymbol{\varepsilon}}^{\boldsymbol{vp}} = |\dot{\varepsilon}^{vp}| \, \frac{3\boldsymbol{s}}{2q} \tag{9}$$

where $q = \sqrt{\frac{3}{2}\boldsymbol{s}:\boldsymbol{s}}$ the Von-Mises shear stress and $|\dot{\varepsilon}^{vp}|$ is the intensity of the creep strain rate, defined by the following double-power law:

$$|\dot{\varepsilon}^{vp}| = A_1^* \left(\frac{q}{q_0}\right)^{N_1} + A_2^* \left(\frac{q}{q_0}\right)^{N_2} \tag{10}$$

where N_1 and N_2 are two stress exponent parameters, while A_1^* and A_2^* are two viscosity-like parameters, which are generally temperature-dependent:

$$\begin{aligned} A_1^* &= A_1 e^{\left(-\frac{Q_1}{R}\frac{1}{T}\right)} \\ A_2^* &= A_2 e^{\left(-\frac{Q_2}{R}\frac{1}{T}\right)} \end{aligned} \tag{11}$$

In which A_1 and A_2 are two reference viscosity parameters, $R = 8.314\, J.mol^{-1}K^{-1}$ is the universal gas constant and Q_1 and Q_2 are two creep activation energy parameters ($J.mol^{-1}$). Since R is a constant independent of material, in practice it is only important to know the values of Q_1/R and Q_2/R as two constitutive parameters. Note that in (11) T **must be the absolute temperature** (in Kelvin unit).

Note that in the standard form of the empirical Norton's law (1) the unit of the viscosity-like parameter A is "material dependent" and a bit confusing. In the current formulation (10) the reference stress q_0 is used to render the stress term under the exponents $\frac{q}{q_0}$ dimensionless, and thereby to get a proper and clearer unit for the viscosity-like parameters A_1 and A_2 (*1/time unit*). Depending on the context (range of stress value, calibration process of model parameters in laboratory etc.), q_0 may be taken for instance 1 MPa or 100 kPa (atmospheric pressure). Certainly, this reference stress q_0 can take any other positive value, but the model parameters A_1 and A_2 should be modified correspondingly.

2.3 N2PC-MCT model: an extended version of N2PC with Mohr-Coulomb and Tension cut-off failure criterion

As aforementioned, the N2PC-MCT model combines the original N2PC presented above with the Mohr-Coulomb and Tension cut-off failure criterion. Concretely, the strain decomposition (3) is extended as follows:

$$\boldsymbol{\varepsilon} = \boldsymbol{\varepsilon}^{\boldsymbol{e}} + \boldsymbol{\varepsilon}^{\boldsymbol{T}} + \boldsymbol{\varepsilon}^{\boldsymbol{vp}} + \boldsymbol{\varepsilon}^{\boldsymbol{p}} \tag{12}$$

The first 3 components (elastic strain $\boldsymbol{\varepsilon^e}$, thermal strain $\boldsymbol{\varepsilon^T}$, viscoplastic creep strain $\boldsymbol{\varepsilon^{vp}}$) stay the same as in the original N2PC model described earlier (Equations (4)-(11)). The newly added term $\boldsymbol{\varepsilon^p}$ is the time-independent plastic strain characterized by the well-known Mohr-Coulomb model. When the failure criterion, governed by standard strength parameters (cohesion, friction angle, tensile strength), is violated, stress state stays on the yield contour and plastic strain is generated following a perfectly plastic non-associative law (governed additionally by a dilation angle). The detailed presentation of this model can be found in Plaxis Material models Manuals, for instance (Plaxis, 2021)

2.4 Model implementation in PLAXIS

The general (non-isothermal) version of the N2PC and N2PC-MCT model was implemented in Plaxis as 2 User-Defined Soil Models (UDSM). Both models are embedded in the same dynamic link library (dll) file. The models can be used for analysing both the general non-isothermal and isothermal cases (without thermal analysis).

Some main features of the stress integration scheme used for the N2PC model are described hereafter. Assuming that all the values at time "n'' (denoted by a subscript "n"), as well as the time increment Δt_{n+1}, the total strain increment $\Delta\boldsymbol{\varepsilon_{n+1}}$, and the temperature increment ΔT_{n+1} are known. Those incremental values emanate from the general Finite Element calculation of the PLAXIS kernel. The role of the constitutive model is to update correctly the effective stress $\boldsymbol{\sigma_{n+1}}$, which can be classically computed as follows:

$$\boldsymbol{\sigma_{n+1}} = \boldsymbol{\sigma_n} + \mathbb{D}\colon\left[\Delta\boldsymbol{\varepsilon_{n+1}} - \Delta\boldsymbol{\varepsilon^T_{n+1}} - \Delta\boldsymbol{\varepsilon^{vp}_{n+1}}\right] \tag{13}$$

where $\mathbb{D}$ is the elastic stiffness tensor, $\Delta\boldsymbol{\varepsilon^T_{n+1}}$ is the thermal expansion strain increment and $\Delta\boldsymbol{\varepsilon^{vp}_{n+1}}$ the creep strain increment.

As aforementioned, the thermal strain $\Delta\boldsymbol{\varepsilon^T_{n+1}}$ is automatically calculated inside the PLAXIS programs and therefore *not* needed to be considered at the constitutive level. The model aims at evaluating the component $\Delta\boldsymbol{\varepsilon^{vp}_{n+1}}$ which can be computed based on a generalised trapezoidal rule:

$$\Delta\boldsymbol{\varepsilon^{vp}_{n+1}} = \Delta t_{n+1}\left((1-\theta)\dot{\boldsymbol{\varepsilon}}^{\boldsymbol{vp}}_{\boldsymbol{n}} + \theta\dot{\boldsymbol{\varepsilon}}^{\boldsymbol{vp}}_{\boldsymbol{n+1}}\right) \tag{14}$$

with $0 \leq \theta \leq 1$ is a stress integration scheme parameter, while $\dot{\boldsymbol{\varepsilon}}^{\boldsymbol{vp}}_{\boldsymbol{n+1}}$ is the creep strain rate evaluated at the unknown (targeted) stress level $\boldsymbol{\sigma_{n+1}}$. As the creep strain rate is a nonlinear function of stress (see Eq. (10)), the integration (13) is a *nonlinear problem*.

The choice of integration scheme depends on two important criteria: *stability condition* and *accuracy condition*.

For the **stability condition**, it is theoretically demonstrated (Simo & Hughes, 1997) that if $\theta < 1$, namely including both explicit ($\theta = 0$) and Crank-Nicholson scheme ($\theta = 0.5$), only conditional stability is ensured (i.e. time step should be small enough for stability). Only **fully implicit** scheme $\theta = 1$ may guarantee unconditional stability. Such a scheme is therefore chosen in the implementation of the N2PC model:

$$\theta = 1; \quad \Delta\boldsymbol{\varepsilon}^{\boldsymbol{vp}}_{\boldsymbol{n+1}} = \Delta t_{n+1}\dot{\boldsymbol{\varepsilon}}^{\boldsymbol{vp}}_{\boldsymbol{n+1}} \tag{15}$$

In this case of implicit scheme, as $\dot{\boldsymbol{\varepsilon}}^{\boldsymbol{vp}}_{\boldsymbol{n+1}}$ is a function of the unknown stress variable $\dot{\boldsymbol{\varepsilon}}^{\boldsymbol{vp}}_{\boldsymbol{n+1}}(T_{n+1}, \boldsymbol{\sigma}_{\boldsymbol{n+1}})$, a Newton Raphson iteration process is used to solve the nonlinear equation (13) to get the solution of $\boldsymbol{\sigma}_{\boldsymbol{n+1}}$.

For the **accuracy condition**, it is well-known that accuracy is time step-dependent. Both implicit and explicit schemes are first-order accurate, and only Crank-Nicholson schemes are second-order accurate. To ensure the accuracy condition, an **automatic time-stepping** is used, based on the evaluation of the local truncation error inspired by (Mahnken & Stein, 1989). The global time step (which can be very high) is subdivided into smaller time steps to ensure a small enough local error of creep strain within each step integration.

For the N2PC-MCT model, the creep stress solution resulted from the above implementation is served as a trial viscoplastic stress (assuming plasticity strain does not occur during the calculation step). If the trial stress leads to a violation of the failure criterion (Mohr-Coulomb with Tension cut-off), a return-mapping algorithm is used to bring the stress state to the yield contour. Due to the complexity of the nonlinear processes involved (plasticity coupled with viscoplasticity), an additional sub-stepping is implemented to ensure better accuracy.

Note that in general, the time step criterion for accuracy is less restrictive than that for stability criterion. Therefore, even with sub-stepping, implicit scheme allows using much larger time step than explicit scheme. Moreover, *stability condition is generally a property of the system of equation and should be imposed at all the stress points,* whereas *accuracy based time-stepping is only used for the stress points which exhibit high creep responses*. Another remark is that although the above adaptive sub-stepping schemes are proved to be efficient, in some cases especially when both viscoplastic creep and plastic failure are involved, the smoothness and accuracy of the solutions can be improved by reducing the step-size as well as global tolerated error in a Finite Element Analysis.

2.5 Summary of the model

General non-isothermal version of the N2PC model

The general version of the N2PC model allows to model creep responses together with thermal analyses. In this case it consists of 10 parameters (see Figure 2), including:

1. Elastic shear modulus G (*stress unit*) and Poisson's ratio ν (see Eq. (5)-(7)).

2. Creep stress exponents N_1, N_2 (see Eq. (10)). Typical values range from 1 to 8.

3. The viscosity like parameters A_1, A_2 (*1/time unit*, see Eq (11)).

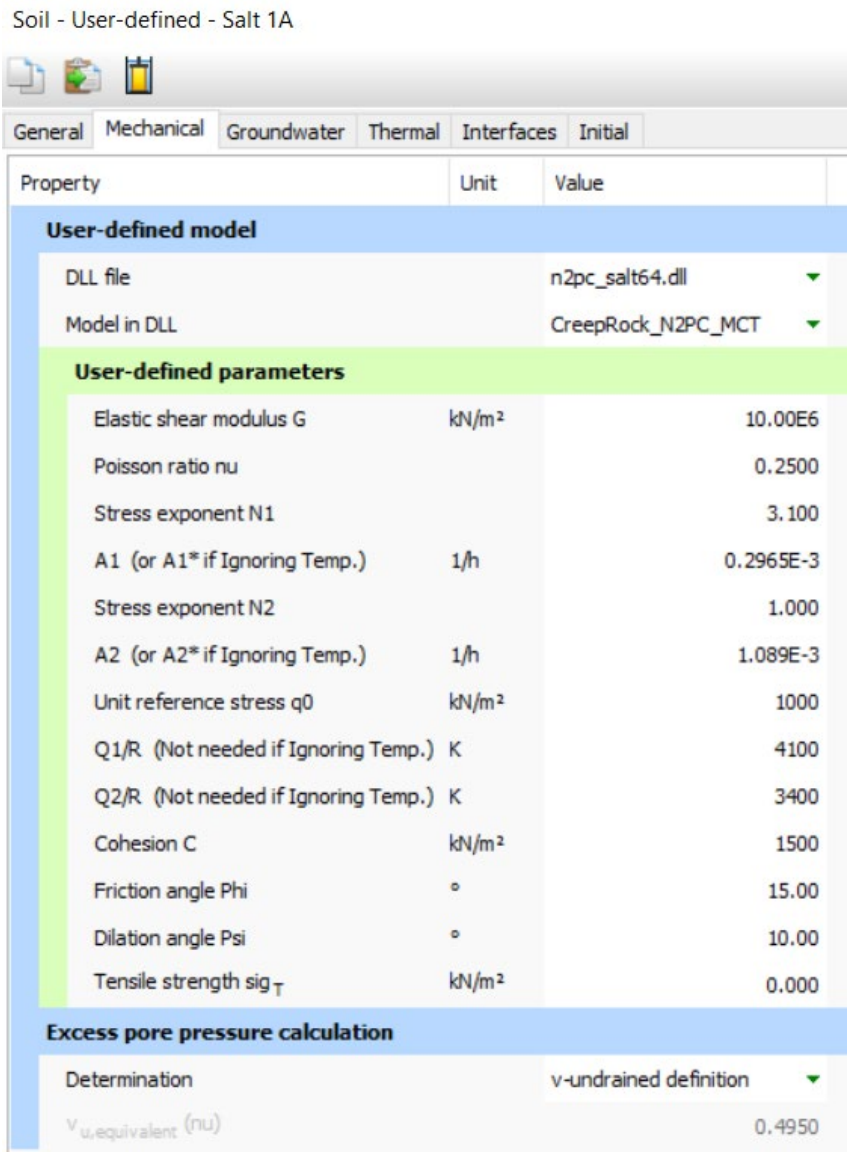

Figure 2 Model parameters User-Interface

4. Thermal-related parameters $\frac{Q_1}{R}, \frac{Q_2}{R}$ (*Kelvin unit*, see Eq (11)).

   ***Remark**: since Eq (11) is only valid for an absolute pressure, $\frac{Q_1}{R}$ and $\frac{Q_2}{R}$ must be always in Kelvin unit. In the PLAXIS project properties, user may use different unit temperature unit (°C or °F) but those material properties will NOT be converted accordingly.*

5. The reference stress parameter q_0 (*stress unit*). As explained earlier, this is not a material constant, but only a parameter to get a proper unit for the parameters A_1, A_2. It is recommended, for simplicity, to choose $q_0 = 1$ unit of stress. However, any other positive value can be chosen for q_0 but A_1, A_2 should be changed correspondingly.

***Example**: if stresses are expressed in MPa, we may choose $q_0 = 1MPa$, i.e the material properties A_1, A_2 are fitted using creep test results for strain rate and the dimensionless stress $\frac{q}{q_0}$. We also may choose for instance $q_0 = 100kPa = 0.1MPa$, but the parameter A_1 and A_2 should be changed to $A_1/(0.1)^{N1}$ and $A_2/(0.1)^{N2}$.*

6. All the parameters should be positive to ensure mathematically and physically realistic results. If negative values are used, an abort message will be displayed and the calculation will be stopped

7. In these particular models, creeping points (the stress points which produce creep strain) are displayed as "Cap points" in PLAXIS Output

Ignoring Temperature Version

The model can also be used *without* thermal analysis. This is where the temperature calculation is ignored (for instance when the temperature change is not significant). In this case, the following points should be considered:

1. The temperature-related parameter $\frac{Q_1}{R}, \frac{Q_2}{R}$ are not needed (see Figure 2). Their values will not affect the calculation results.

2. Only Eq (10) is considered, i.e. the parameters A_1^* and A_2^* are used instead of A_1 and A_2. ***Remark**: although Eq (11) is not explicitly considered in this case, it is implicitly understood that A_1^* and A_2^* are the values evaluated at an assumed constant temperature T_0. The users should provide the correct values for A_1^* and A_2^* at that constant temperature.*

Additional features for the N2PC-MCT model

The N2PC-MCT has all the above parameters of the N2PC model together with 4 additional parameters (see Figure 2), including:

1. Cohesion c and tensile strength sig_T (stress unit). To avoid numerical instability, it is recommended that these values should be larger than zero.

2. Friction φ and Dilation angle ψ (degree unit).

3. The plastic failure points and tensions can be displayed in PLAXIS Output program, together with creep points (shown as cap points as explained earlier)

2.6 Comments and remarks on the theoretical model and its PLAXIS implementation

The constitutive model described in (9) and (10) may apply to simulate the time-dependent responses of rock in general and rock salt in particular.

1. Only *Steady-state Creep* is considered. This is more or less relevant for the time scale considered in underground engineering applications. Although only steady-state creep is considered at the material level, the model may also describe the **"geometrical transient creep" due to stress redistribution** around the cavity as reported in previous works (Bérest, et al., 2017). This will be demonstrated by the numerical example presented in Chapter 4.

2. *No creep threshold* is considered, i.e. creep occurs once deviatoric stresses are non-null. This is more or less consistent with rock salt but also with other rock materials since detecting a stress threshold for creep is not always straightforward in laboratory.

3. *No volumetric creep strain* is considered, i.e. creep is isochoric. This is often observed for rock salt.

4. The creep rate is increased with the temperature. Note that in (10) the temperature T must be the *absolute temperature* (in Kelvin unit).

5. The creep law is an extension of the original Norton's law with 2 power branches. This provides more flexibilities allowing to better reproduce the rock behaviour (Gunther, et al., 2015). In particular, rock salt exhibits different responses at low and high stress levels. At low stresses, pressure-solution mechanism is dominant (which can be described by a "linear" power law with the exponent equal to unity) (Fokker, 1994). At higher stresses (for instance, higher than 5 MPa) dislocation mechanism governs creep behaviour and a higher value of stress exponent should be used (Berest, et al., 2012) (Gunther, et al., 2015).

6. A robust and efficient implementation was performed with a *fully implicit scheme* with an *automatic local sub-incrementing* procedure. This allows to use a relatively large time step, and only sub-step at the points of the structure that are subjected to significant creep loading to satisfy accuracy condition.

7. *This UDSM is developed compatible with PLAXIS 3D 2018 and PLAXIS 2D 2019 or later versions. When using older versions, please only use **exclusively Kelvin unit** and set* $\frac{Q_1}{R} = \frac{Q_2}{R} = 0$ *for Ignoring Temperature Version*

8. *Compared to N2PC-MCT, the N2PC model has less parameters and is useful for deformation analysis, especially when only the long-term deformation is of primary importance. By setting the strength parameters (concretely cohesion c and tensile strength sig_t) to very high values so that plastic failure cannot be reached, N2PC-MCT model would coincide with N2PC model*

3 Model Verifications

Some basic tests are presented in this Section to verify the model implementation, for different Plaxis products, including: PLAXIS 2D (2019); PLAXIS 3D (2018); and SoilTest facility. They are based on the simulation of typical *homogenous* laboratory tests (with simple geometry).

The unit of time is set to *hours* that of temperature is set for *°C*. The stress unit is chosen as *kPa*. The creep parameters were calibrated based on stresses results in MPa unit, therefore the unit reference stress parameter is chosen $q_0 = 1\ Mpa = 1000\ kPa$

To run the model, the file N2PC64.dll containing the CreepRock_N2PC model is placed in the UDSM sub-folder of the PLAXIS program directory.

Let's consider 2 rock salts with the same material properties except for creep parameters. The other parameters are presented in Table 1.

Parameters	**Salt 1**		**Salt 2** *(constant strain rate test)*
	Salt 1A *(general non-isothermal analyses)*	***Salt 1B*** *(ignoring temperature analyses)*	
Shear modulus G	10 GPa		
Poisson's ratio ν	0.25		
1st Creep exponent N_1	3.1		2
1st Creep parameter A_1	2.965 10^{-4} 1/h	$A_1^* = 0.25\ 10^{-9}$ 1/h	11.86 10^{-3} 1/h

2nd Creep exponent N_2	1		-
2nd Creep parameter A_2	1.089 10^{-3} 1/h	$A_2^* = 1\ 10^{-8}$ 1/h	0
1st Temp.-related term $\frac{Q_1}{R}$	4100 K	-	4100 K
2nd Temp.-related term $\frac{Q_2}{R}$	3400 K	-	3400 K
Cohesion C	1500 kPa	1500 kPa	5000 kPa
Friction angle Phi	15^0	15^0	40^0
Dilation angle Psi	10^0	10^0	10^0
Tensile strength sig_T	100 kPa	0 kPa	0 kPa

Table 1. Parameters for verification examples

The parameter for **Salt 1** is chosen in agreement with rock salt experimental data, the creep behaviour is typically described by 2 branches. The first branch represents dislocation creep and is modelled by a power law with a typical value of the exponent $N_1 = 3.1$. The second represents pressure-solution creep (dominant at low stress level) and can be modelled by a linear law, i.e., $N_2 = 1$. To illustrate different use of the model implemented in PLAXIS, 2 material sets are considered based on the same material properties of Salt 1. The *Salt 1A* includes all the material properties of Salt 1, which can be used for general non-isothermal analyses. The second set for *Salt 1B* corresponds to the creep parameters of Salt 1 at 20°C which is used when temperature calculation is ignored. Temperature related parameters $\frac{Q_1}{R}, \frac{Q_2}{R}$ are not needed. Moreover, as explained before, A_1^* and A_2^* are needed instead of A_1, A_2. In this case, they may be estimated at 20°C based on (11) using the data of $A_1, A_2, \frac{Q_1}{R}, \frac{Q_2}{R}$. For **Salt 2**, only one branch of creep power is considered. This is only to facilitate the comparison against analytical solution for constant strain rate testing, where closed-form solution is only obtained for single power law with $N_1 = 2$. This can be explained in detail in Section 3.3.

Note that to facilitate comparisons, gravity effect is ignored by setting the density equal to zero. Furthermore, all the materials are drained, and no water pressure effect is taken into account in these tests.

3.1 Unconfined uniaxial relaxation test ignoring temperature calculation

Uniaxial relaxation test is simulated without considering temperature analysis, i.e., for **Salt 1B**. This option can be used for both PLAXIS2D, PLAXIS 3D and SoilTest facility.

General description and Closed form solution

The sample is subject to an initial elastic loading ε_1^{ini} corresponding to an initial stress values $\sigma_1^{ini} = -q^{ini}$ where "1" indicates the loading axis. The configuration of the uniaxial test allows to write the relationship between the applied axial stress $q = -\sigma_1$ and the axial strain as follows:

$$\dot{\sigma}_1 = E(\dot{\varepsilon}_1 \ - \dot{\varepsilon}_1^{vp}) \tag{16}$$

where $E = 2G(1 + \nu)$ is the Young's modulus.

	Loading (Strain) condition	Loading (Time) condition
Instantaneous Loading Phase	$\varepsilon_1^{ini} = -0.04\%$	0 hours
Relaxation phase	$\dot{\varepsilon}_1 \ = 0$	30000 hours

Table 2. Loading condition for unconfined relaxation test on rock material

The relaxation condition $\dot{\varepsilon}_1 \ = 0$, and the creep constitutive equations (9) and (10) allow to rewrite (16):

$$\dot{q} + E\left[\left(\frac{A_1^*}{q_0^{N_1}}\right)q^{N_1} + \left(\frac{A_2^*}{q_0^{N_2}}\right)q^{N_2}\right] = 0 \tag{17}$$

In the case where $N_2 = 1$, some mathematical techniques (see for instance (Polyanin & Zaitsev, 2017)) allow to solve analytically the nonlinear ordinary differential equation (17) to get the evolution of the axial deviatoric stress:

$$q = \left[\left[\left(q^{ini}\right)^{1-N_1} + \frac{A_1^*}{A_2^*}q_0^{1-N_1}\right]e^{-\frac{(1-N_1)EA_2^*t}{q_0}} - \frac{A_1^*}{A_2^*}q_0^{1-N_1}\right]^{\frac{1}{1-N_1}} \tag{18}$$

The corresponding PLAXIS models are performed. The general loading condition is provided in Table 2. During the loading phase, an instantaneous strain of 0.04% is applied corresponding to a theoretical initial stress. For the N2PC model, this initial stress corresponds to an elastic stress of 10 MPa, while for the N2PC-MCT model, this stress corresponds to a plastic uniaxial strength, and can be calculated by:

$$q^{ini} = \frac{2c\ cos\ (\varphi)}{1 - sin\ (\varphi)} \tag{19}$$

This stress is expected to be relaxed during the relaxation phase which lasts 30000 hours following Eq. (18).

SoilTest Simulation

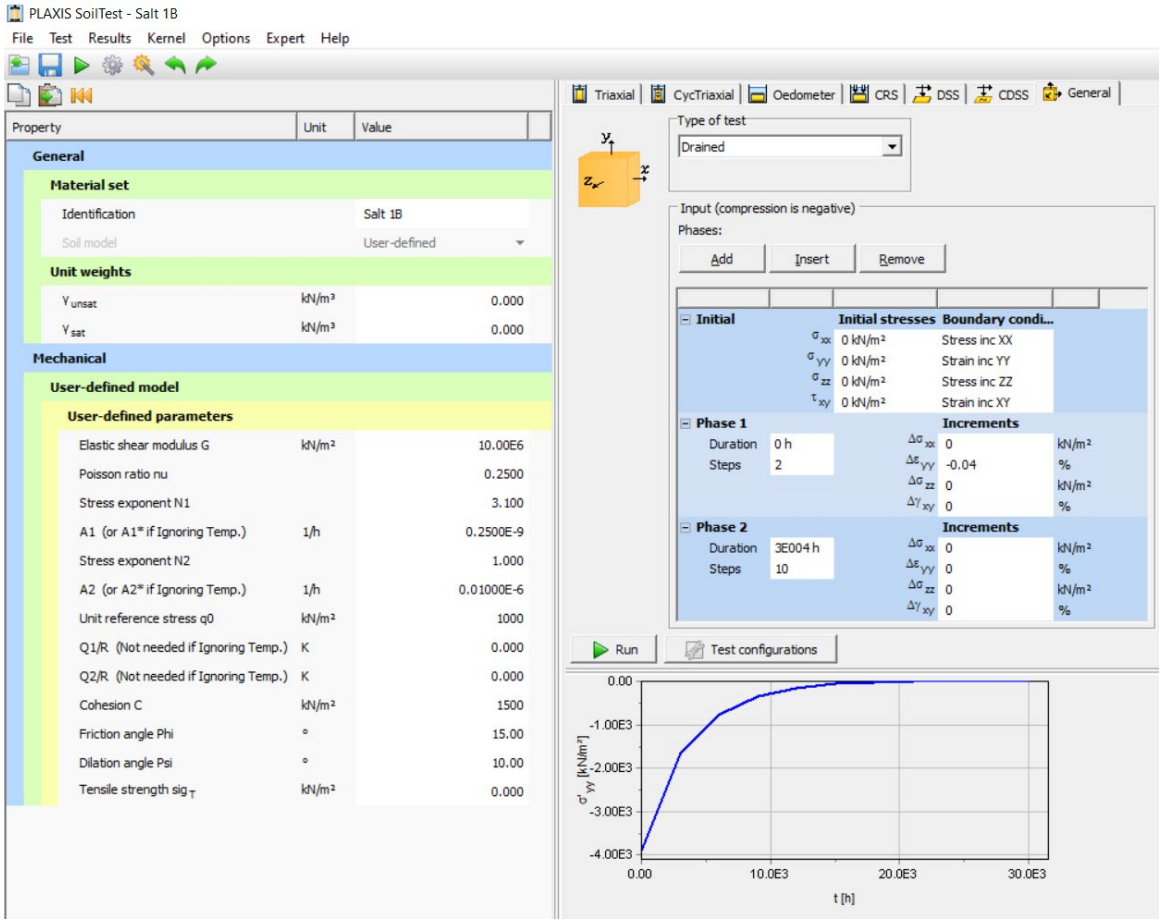

Figure 3 Modelling of unconfined relaxation test by SoilTest facility of Plaxis

The SoilTest simulation is simply based on stress calculation without any geometry effect. The relaxation test configuration can be defined in the General Test type. 2 Steps were used for the instantaneous loading phase, while only 10 time steps to simulate the relaxation phase, which lasts for a very long time (30000 hours, namely around years). The typical result of the relaxation test is often expressed by plotting a stress – time graph. This can be done by *Right click → add custom chart* in the SoilTest User Interface (Figure 3).

PLAXIS 2D simulation

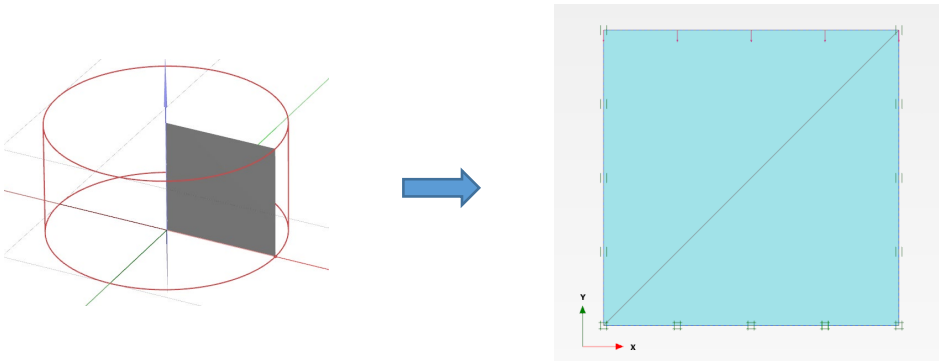

Figure 4. Modelling of unconfined relaxation test by PLAXIS 2D: Axisymetric model mesh and boundary conditions

PLAXIS The same test was simulated using PLAXIS 2D program. An axisymmetric 2D model was built to represent the test condition. The model is 1mx1m in the XY plan. The boundary conditions are: fixities at the left side (symmetry axis of the sample) and at the base of the model, and an imposed displacement equal to $0.4\ 10^{-3}$m (corresponding to $\varepsilon_1^{ini} = 0.04\%$) at the top to represent the loading condition (Table 2). Only 2 elements are needed for this test (Figure 4). The *Plastic calculation type* is chosen together with *ignore temperature* mode. The other options keep their default values.

PLAXIS 3D simulation

PLAXIS 3D program can also be used for simulating the triaxial stress state of the test. Considering the *homogenous stress state characteristic* of the test, a cubic sample is modelled. The boundary conditions and mesh are shown in Fig 3. A surface displacement equal to $0.4\ 10^{-3}$m is applied at the upper boundary of the model. The base of the model is vertically fixed. Due to symmetry, the left and back sides are normally fixed (i.e. fixed in the direction perpendicular to their plane), while the other boundaries are free due to the unconfined condition of the test.

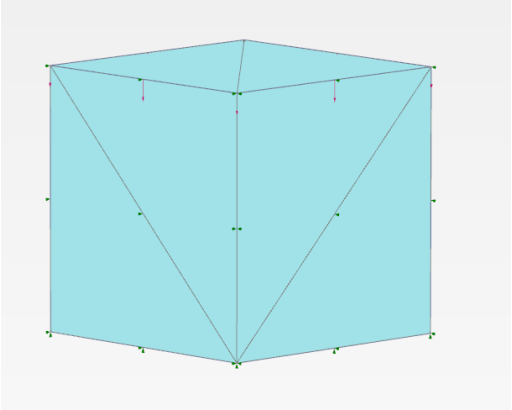

Figure 5. Modelling of unconfined relaxation test by PLAXIS 3D: Model mesh and boundary conditions

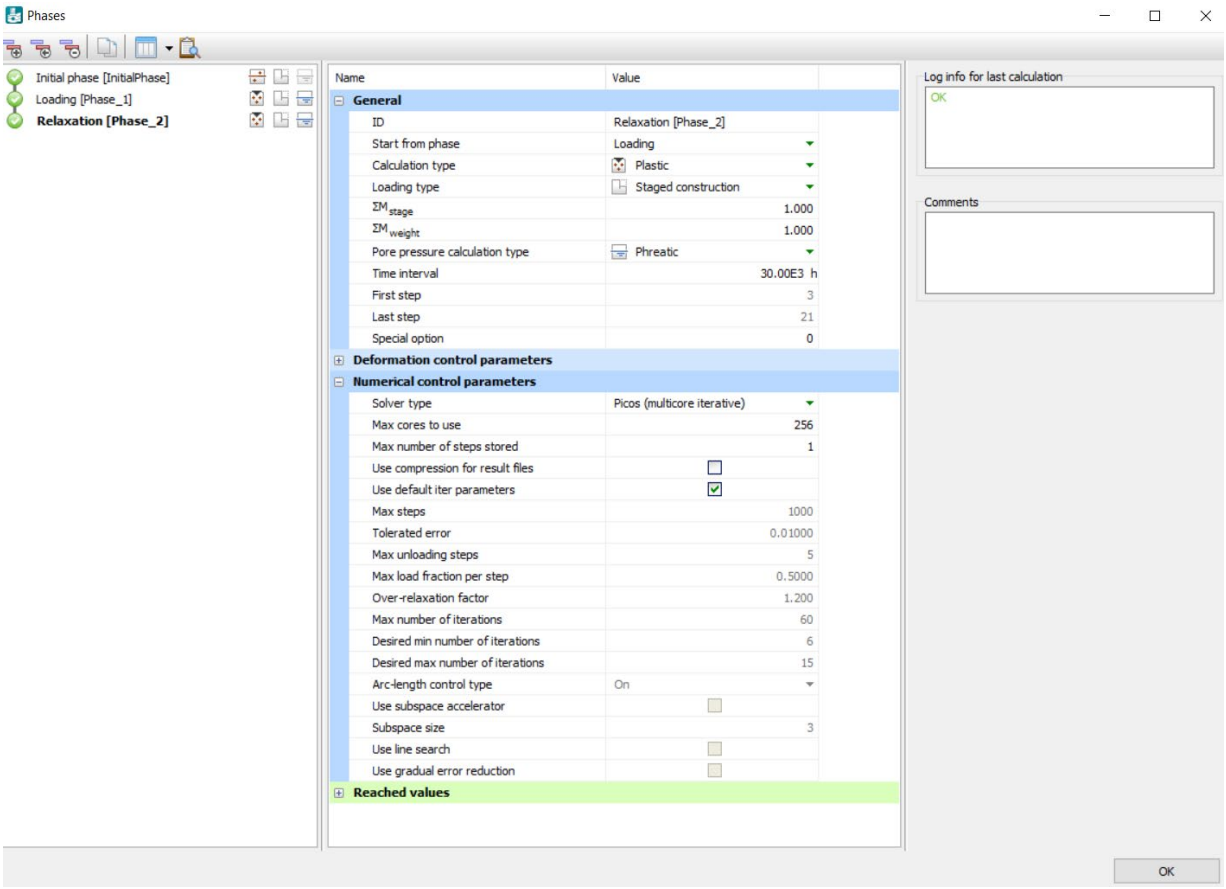

Figure 6. Modelling of unconfined relaxation test by PLAXIS 3D: Calculation Type

The *Plastic calculation type* is chosen with the default automatic time stepping option. For PLAXIS 3D program, no thermal analysis option is available (Figure 6).

Results comparisons

The typical results for stress-time relationship in the relaxation test obtained from different simulations are compared (Figure 7). It is readily seen that all the simulations provide accurate results compared with the analytical solution both for the instantaneous loading phase as well as for the relaxation phase (18).

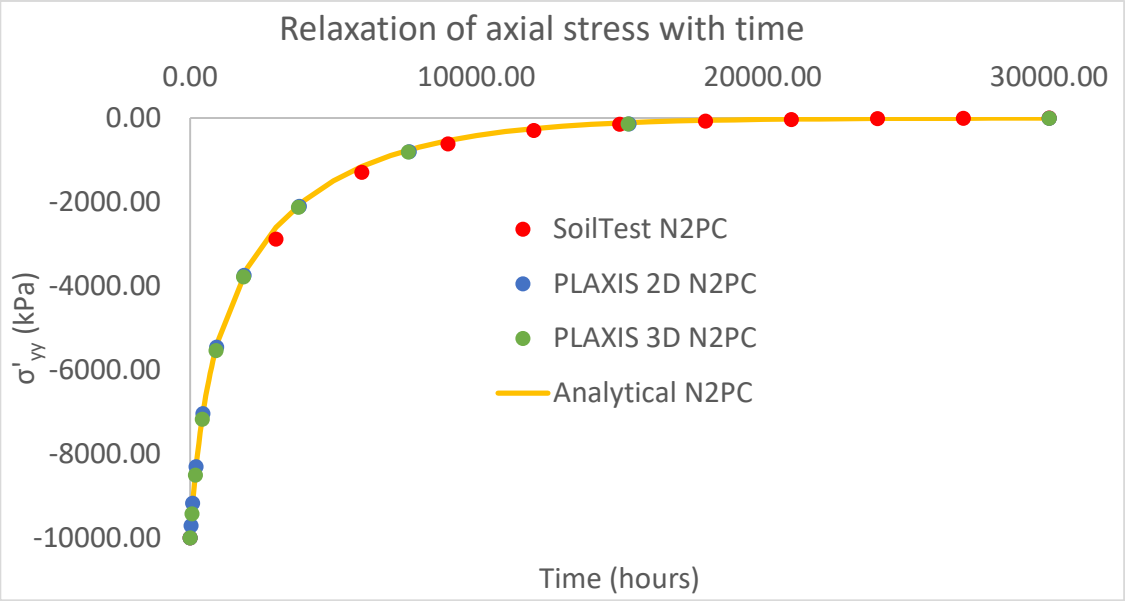

(a)

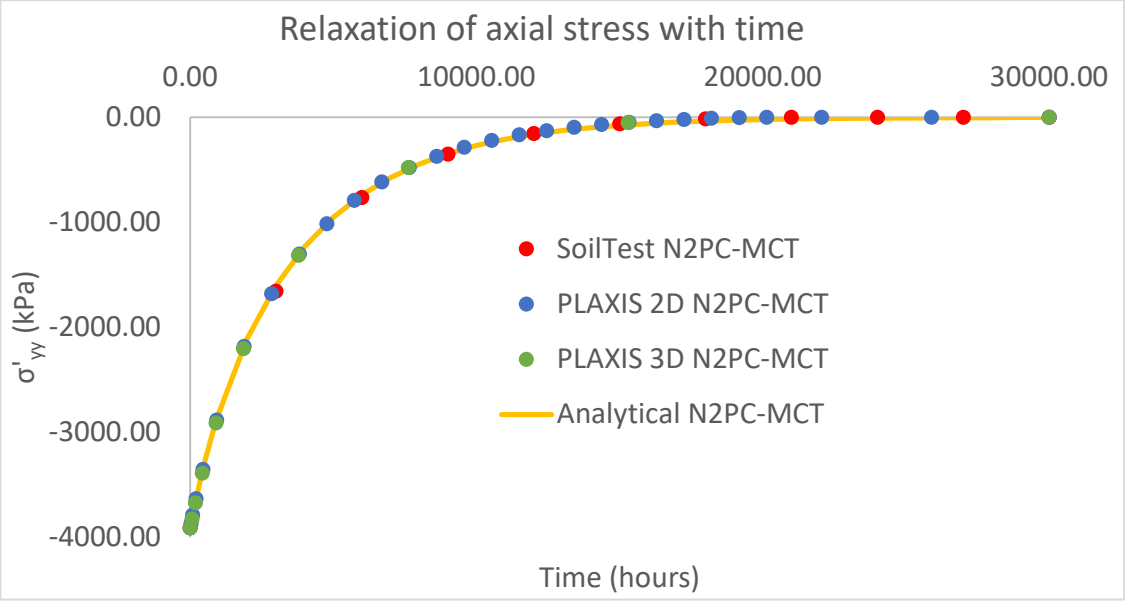

(b)

Figure 7. Stress relaxation curve in Unconfined relaxation test: Comparisons of simulation results by SoilTest, PLAXIS 2D and PLAXIS 3D versus Analytical solution

Moreover, only a small number of time steps (around 10 steps) are needed to get this accurate result. All the time-stepping processes are automatic and very practical. This illustrates the robustness of the implementation.

3.2 Unconfined uniaxial relaxation test at different temperatures

Now to illustrate the thermal effect included in the model, the same test configuration is repeated accounting for different (constant) temperatures. Simulations are made by means of PLAXIS 2D, which is equipped with Thermal module.

In this case the closed form solution (18) is still valid, but Equation (11) is also involved to enable the temperature dependency.

PLAXIS 2D simulations with thermal effect

The parameter set Salt 1A (Table 1) is used to simulate the relaxation tests at 20°C (1st test) and 80°C (2nd test). The full data of $A_1, A_2, \frac{Q_1}{R}, \frac{Q_2}{R}$ are needed. A constant temperature is generated during the Initial phase via Earth Gradient Mode imposed in *Model Condition* (Figure 8).

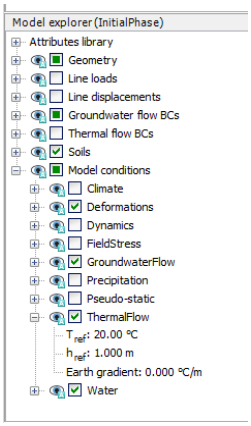

Figure 8. Earth Gradient imposed in Initial Phase of the Test

For the loading phase and the relaxation Phase of the first test, Plastic calculation mode is used in combination with *Use Temperature from Previous Phase* (Figure 9), namely a constant temperature of 20°C is applied.

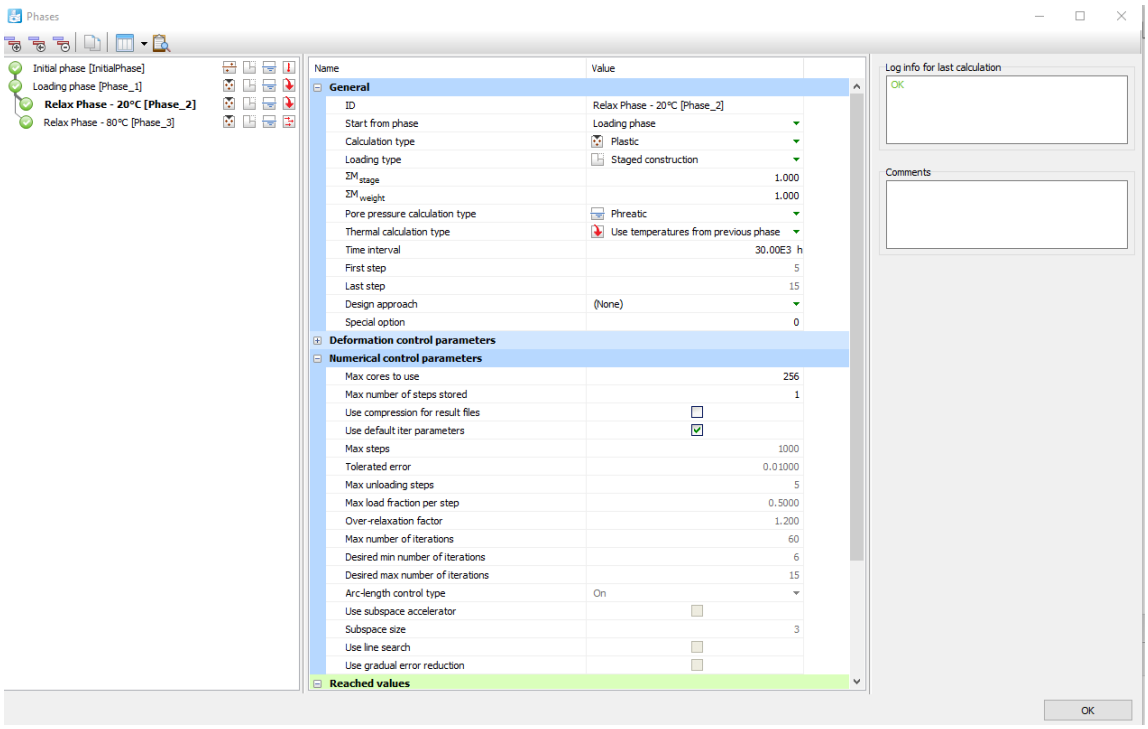

Figure 9. 1st relaxation test uses previous temperature, corresponding to 20°C

The test is then repeated at another temperature of 80°C (during Phase 3, which starts from the Loading Phase). There exist several methods to impose the new temperature value. For instance, a temperature boundary condition is applied on the lower boundary of the model during this phase (Figure 10) together with *Steady-State thermal flow* calculation (Figure 11).

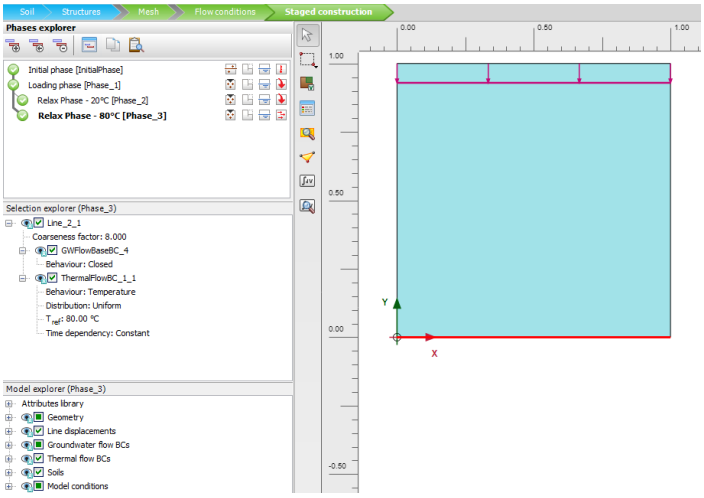

Figure 10. Temperature boundary condition of 80°C applied during Phase 3 (2nd test).

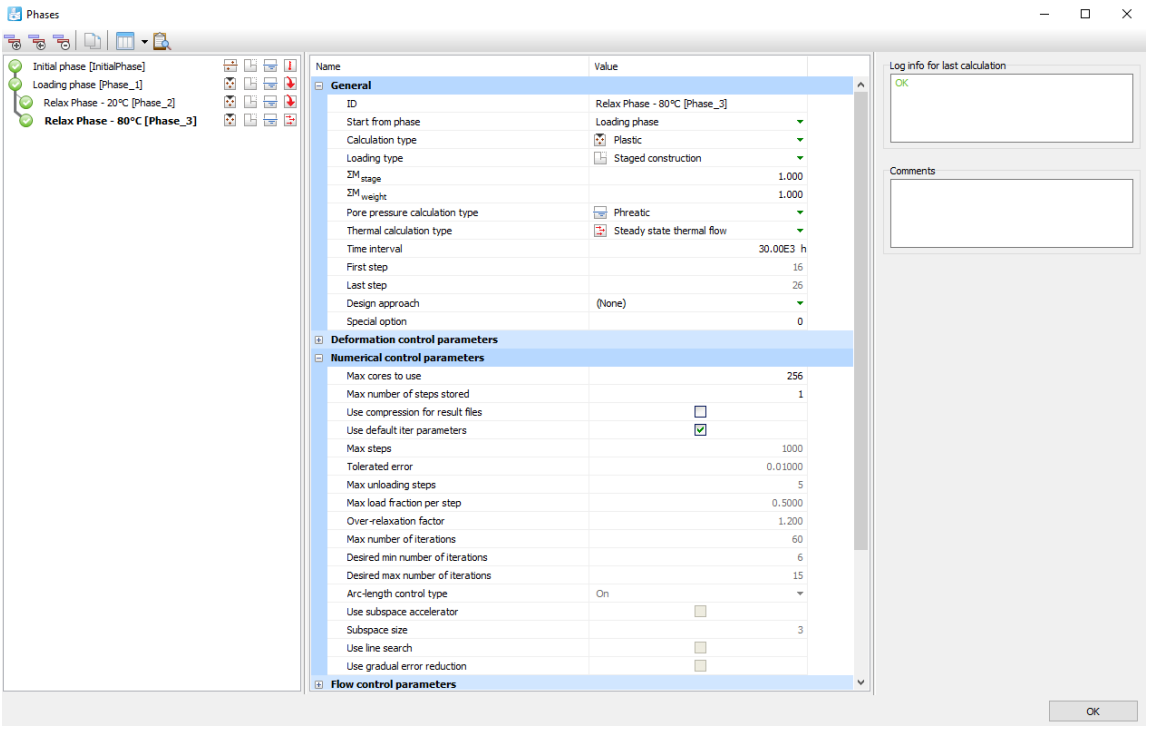

Figure 11. Calculation type for the 2nd relaxation test at 80°C

***Remark**: Note that this Steady-State Thermal calculation results in a **steady-state temperature profile** which is then applied to Mechanical (Plastic) analysis as **a constant input**. This can be verified by checking the temperature results during this phase (*Figure 12*). Precise transient evolution of the temperature coupled with mechanical responses can only be analysed using Fully-Coupled mode. In our basic tests, this mode will result in non-homogenous stress state which is difficult to interpret and compare with analytical results. This is thus not used in these simulations.*

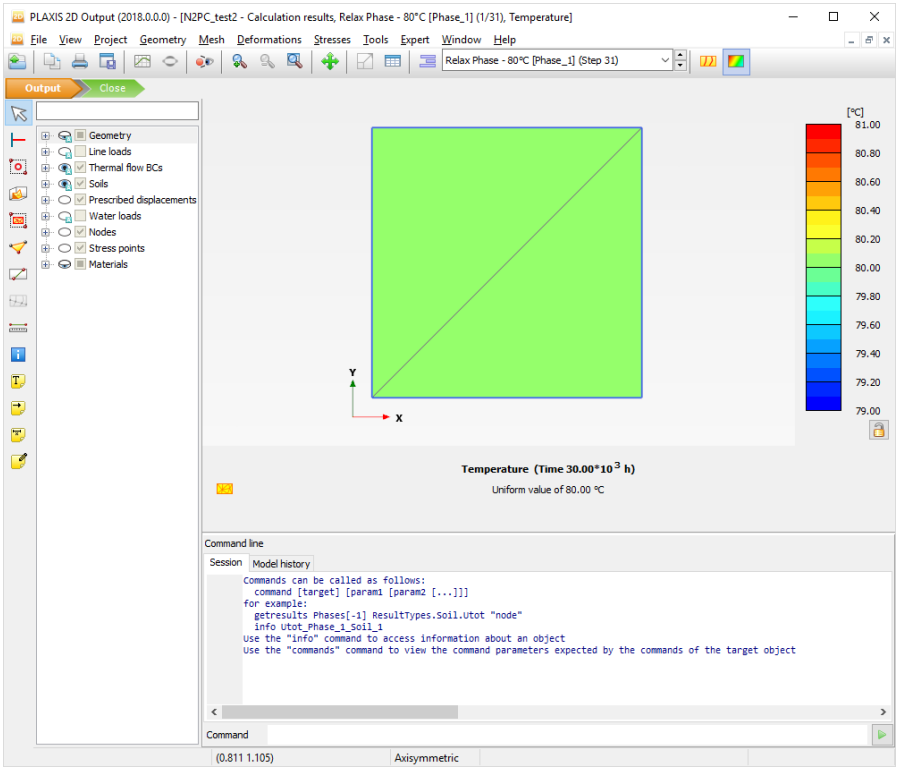

Figure 12. Steady-State Temperature results

Results comparisons

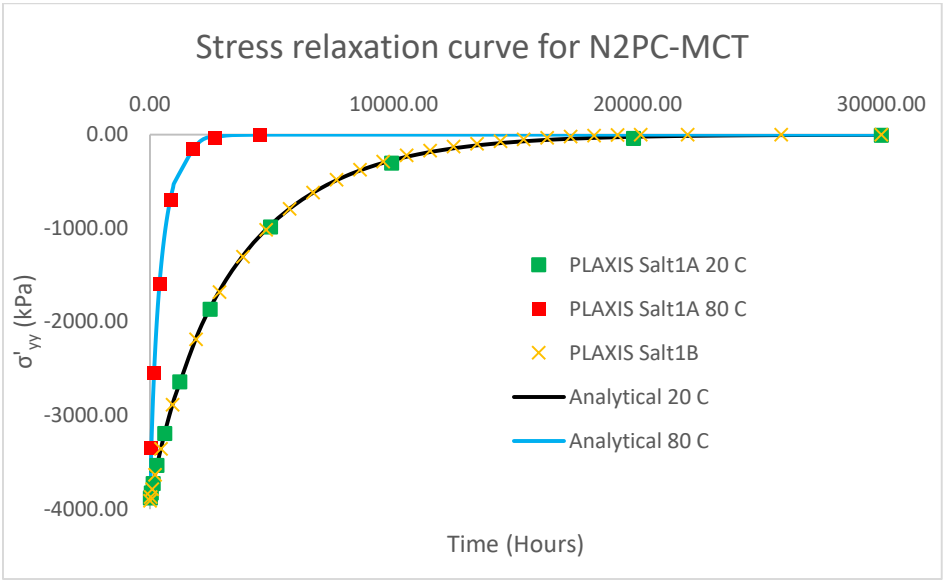

Figure 13. Stress relaxation curve in unconfined relaxation tests at 20°C and 80°C

Again, the typical results for stress-time relationship in the relaxation test obtained from different simulations are compared (Figure 13). It is readily seen that all the simulations provide accurate results compared with the analytical solution (18) together with Condition (11). An increase of temperature leads to an increase of the relaxation rate. Moreover, the simulation result using Salt 1A at 20°C coincides with that obtained previously using Salt 1B as expected (because Salt1B corresponds indeed the reference temperature of 20°C).

3.3 Constant strain rate unconfined compression test at different temperatures

General description and Closed form solution

Constant strain rate test on rock salt sample (at constant temperature) is now simulated. This test is commonly used to study the long-term time-dependent behaviour of rocks (Hudson, 1993). The test configuration is similar to the above unconfined relaxation test. However, the sample is now subject to a constant strain rate $\dot{\varepsilon}_1 = -V_{def} < 0$ (negative sign for compression) during the whole phase to reach a desired strain level. Equation (16) is still valid, but the test condition is $\dot{\varepsilon}_1 = V_{def} = const$ instead of $\dot{\varepsilon}_1 = 0$. The governing ordinary differential equation (17) becomes:

$$\dot{q} + E\left[\left(\frac{A_1^*}{q_0^{N_1}}\right) q^{N_1} + \left(\frac{A_2^*}{q_0^{N_2}}\right) q^{N_2}\right] = EV_{def} \tag{20}$$

This ***non-homogenous nonlinear*** equation is not easy to solve for arbitrary values of N_1 and N_2. This normally requires advanced techniques which may provide closed form but cumbersome results. The general solving is out of the scope of this report, which aims at verifying our model implementation. Therefore, we only take into account the case where only one power-component is active by setting $A_2^* = 0$, and the active component has the power exponent $N_1 = 2$. The simplified equation can be rewritten as follows:

$$\frac{dq}{q^2 - \left(q_0\sqrt{\frac{V_{def}}{A_1^*}}\right)^2} = -E\left(\frac{A_1^*}{q_0^2}\right) dt \tag{21}$$

The integration technique provides the solution, assuming that the initial value $q^{ini} = 0$:

$$q = q_0\sqrt{\frac{V_{def}}{A_1^*}}\left(1 - \frac{2}{1 + e^{\frac{2Et}{q_0}\sqrt{V_{def}A_1^*}}}\right) \tag{22}$$

Note that A_1^* is temperature-dependent via (11).

For the case of N2PC-MCT due to the existence of the Mohr-Coulomb failure envelope the shear stress computed in equation (22) is limited to a uniaxial strength,

$$q_{lim} = \frac{2c\ cos\ (\varphi)}{1 - sin\ (\varphi)} \tag{23}$$

PLAXIS 2D simulations with thermal effect

The test can be simulated without considering temperature dependency using both PLAXIS 2D, PLAXIS 3D and SoilTest facility. Nonetheless, to clarify the temperature effect, PLAXIS 2D simulations with temperature option were conducted. The Salt 2 material parameters (Table 1) are used (see Figure 14).

Four tests are simulated for 2 different strain rates at 2 different temperatures of 20°C (Table 3). The desired total strain level to be reached during the tests is 1%. To this end, a displacement of -0.01 m is imposed in the upper boundary of the sample (Figure 15).

	Strain rate	Temperature
Test 1	$V_{def} = 10^{-3}\ hour^{-1} = 2.78\ 10^{-7} s^{-1}$	20°C
Test 2	$V_{def} = 10^{-4}\ hour^{-1} = 2.78\ 10^{-8} s^{-1}$	20°C
Test 3	$V_{def} = 10^{-3}\ hour^{-1} = 2.78\ 10^{-7} s^{-1}$	60°C
Test 4	$V_{def} = 10^{-4}\ hour^{-1} = 2.78\ 10^{-8} s^{-1}$	60°C

Table 3. Testing condition for 4 constant strain rate compression tests

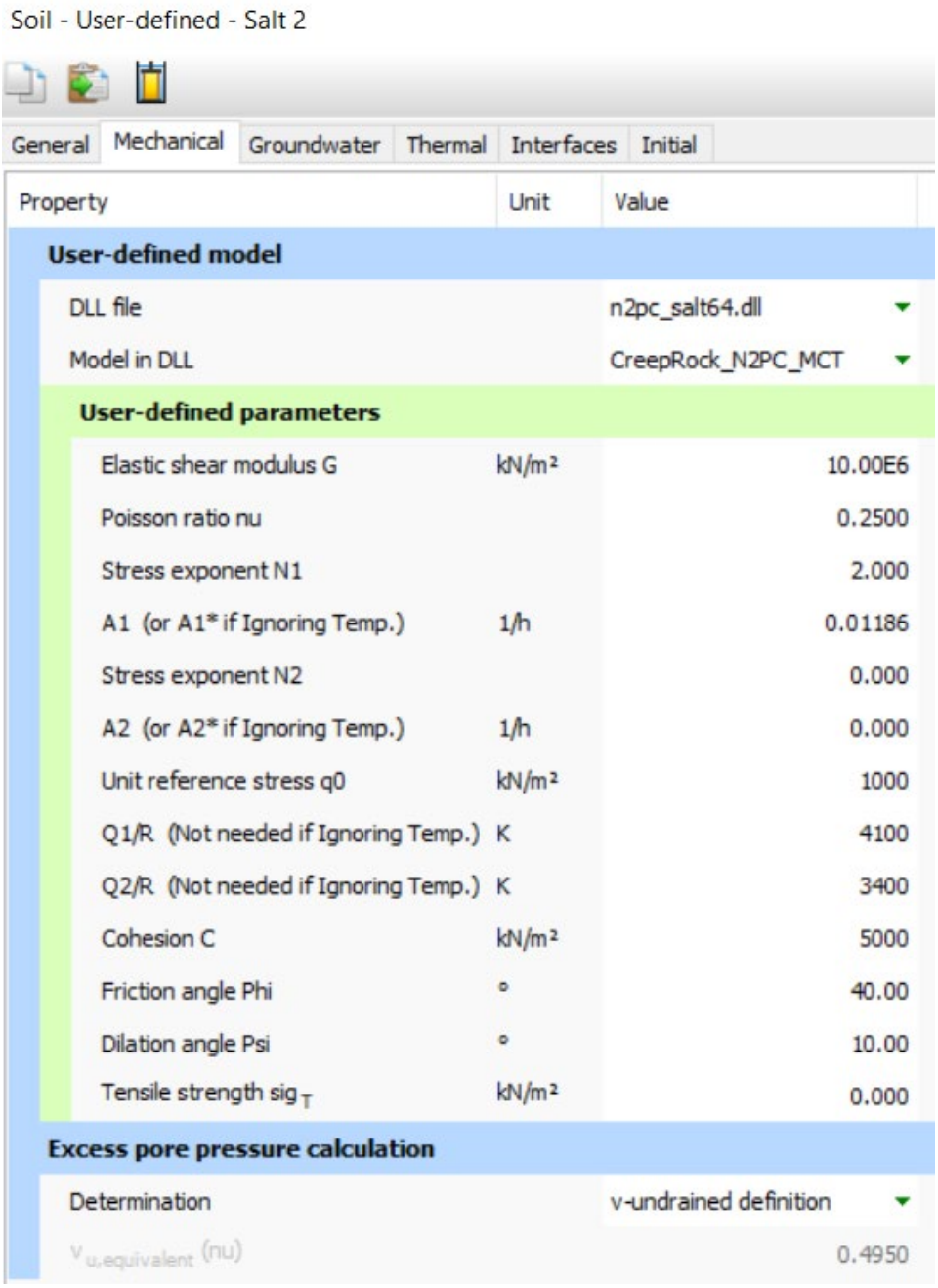

Figure 14. Model Parameters of Salt 2 for constant strain rate tests

Apart from the steady-state thermal flow option presented in Section 3.2, other methods may be used to generate a constant temperature in a cluster. In this example, the temperature of 20°C is generated on Test 2 by assigning a uniform temperature profile in *Thermal Condition* then using *earth gradient* type together with *Plastic calculation* (Figure 16).

In PLAXIS, the desired strain level is reached at the end of the phase with an assumed *linear variation*. The time interval of each test is thus deduced corresponding to each constant strain rate. For example, the test with strain rate of $10^{-4}\ hour^{-1}$ lasts for 100 hours to reach the desired total strain level (Figure 16).

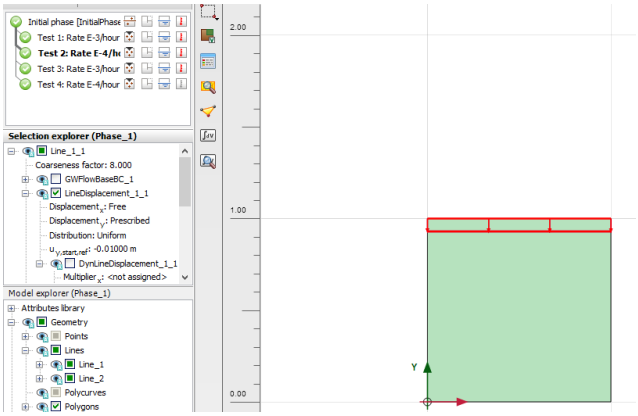

Figure 15. Applied displacement on the sample

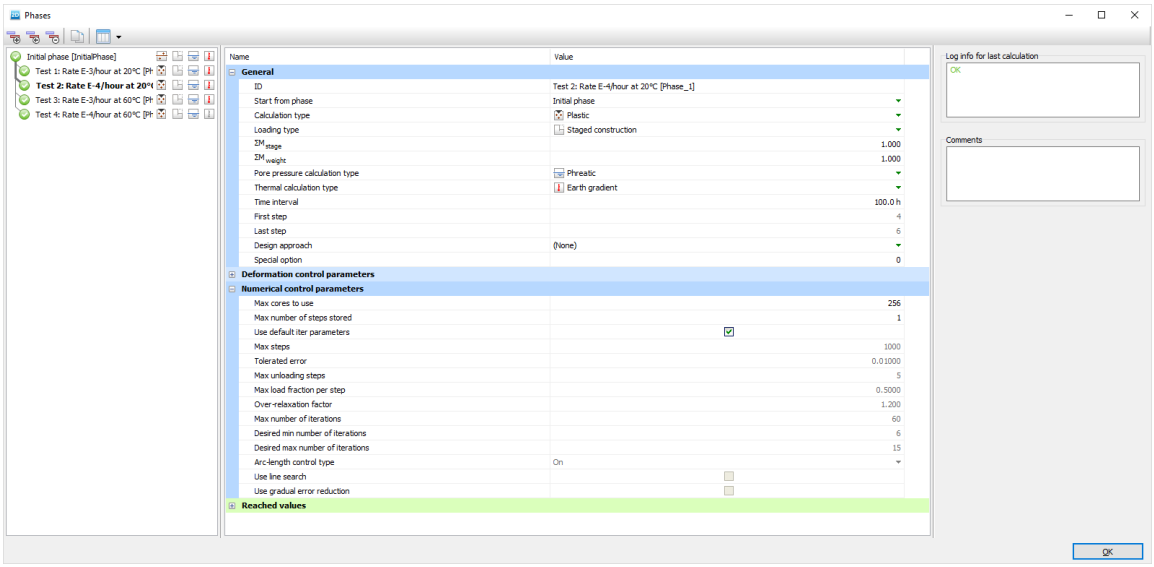

Figure 16. Calculation option setting for Tests 1 and 2

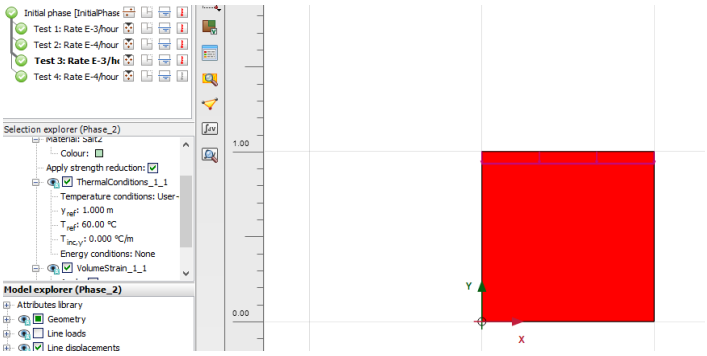

Figure 17. Thermal condition to generate a uniform temperature of 60°C in the sample

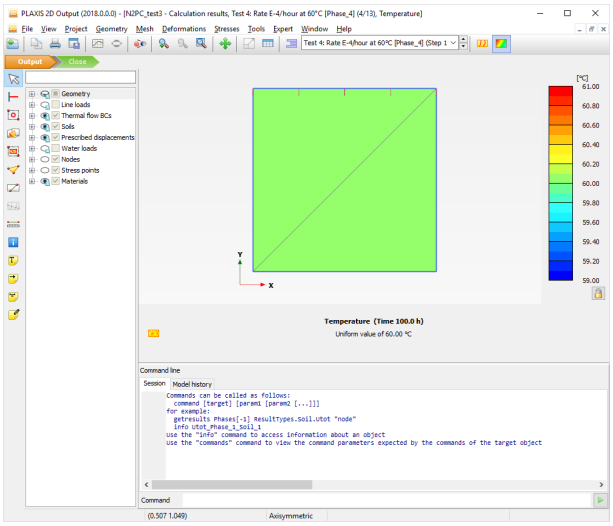

Figure 18. Temperature result for test 4

Another way to apply a temperature to a cluster is to set directly the *temperature condition* of a soil entity. This way is used to impose the temperature of 60°C on our tests 3 and 4 (see Figure 17). Note that this condition setting has a higher priority than Earth Gradient attribute. The generated temperature can be verified when viewing the temperature result (Figure 18).

Results comparisons

The comparisons between the PLAXIS results and analytical solutions (22) together with (11) are carried out and shown in Figure 19. A perfect agreement between the analytical and numerical results is obtained. Both results illustrate the physical processes considered in the N2PC model: creep effect is small for a fast loading, while nonlinear deformation may develop during a slow loading, and these nonlinear strains are enhanced with a higher temperature. For the N2PC-MCT model: a perfect plasticity is observed as expected. Once failure is reached, deformation develops while stress state is limited at material strength level.

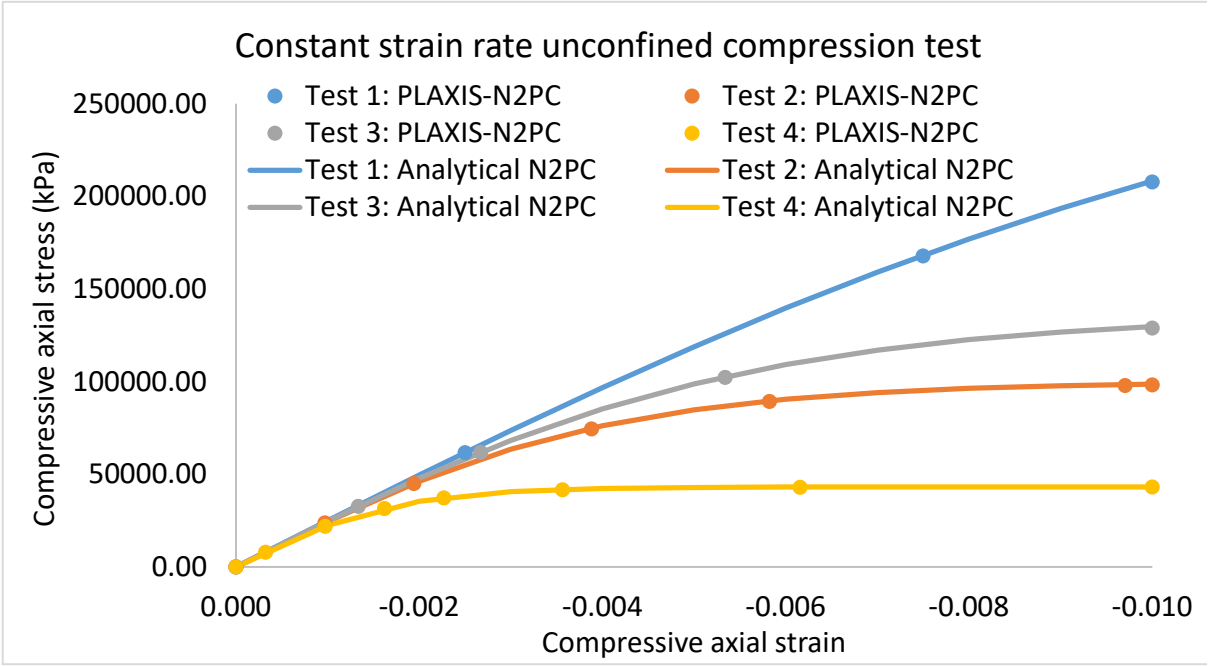

(a)

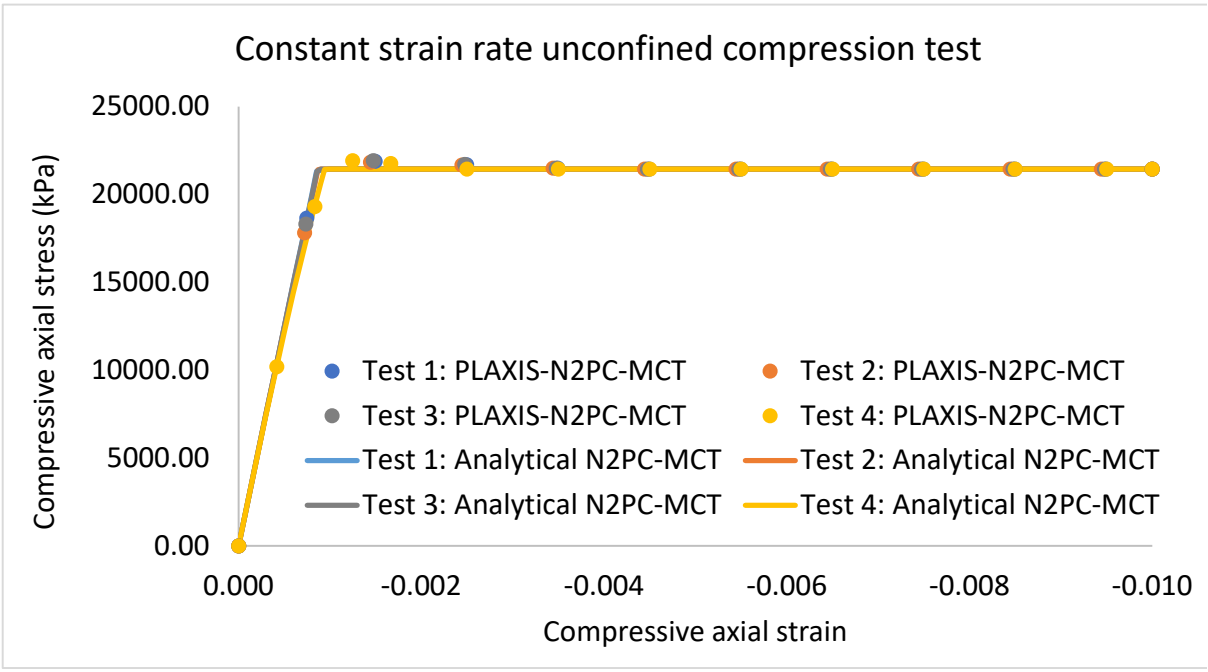

(b)

Figure 19. Comparison between PLAXIS 2D and Analytical results for 4 constant strain rate tests

4 A case study on a salt cavern for hydrocarbon storage

In the following, a case study on a typical deep Compressed Air Energy Storage (CAES) will be examined. An underground cavern for gas storage, excavated in a deep Salt Layer, is simulated during its operation state.

In general, CAES caverns are created by solution mining. Soft water is injected through a cemented well into a salt layer. Rock salt dissolves in water to create a cavern filled with brine, which will be replaced by compressed air used in energy production. Seasonal exploitations of the stored gas consist of gas withdrawal and injection, relating to depressurisation/repressurisation as well as heating/cooling cycles (Bottcher, et al., 2017).

Modelling the whole life cycle of the cavern involves complex coupled phenomena such as rock dissolution (normally from the bottom to the top of the cavern), heat exchanges between gas, brine and rock mass, thermodynamic effects of fluids and mechanical behaviour of the rock mass (creep) (Berest, 2011).

In the following, we simulate the behaviour of a salt cavern subject to a depressurisation process. The solution mining, which can be considered relative short compared to the operation period of the storage, is not modelled. Instead, it is only represented by an initial stress state, assuming that during that short time, stress redistribution due to creep does not occur significantly. We also follow a very common assumption that rock salt is non-porous and only thermo-mechanical coupling is taken into account (Zhu, et al., 2017) (Berest, et al., 2012) (Fokker, 1994) (Bottcher, et al., 2017).

4.1 Model definition

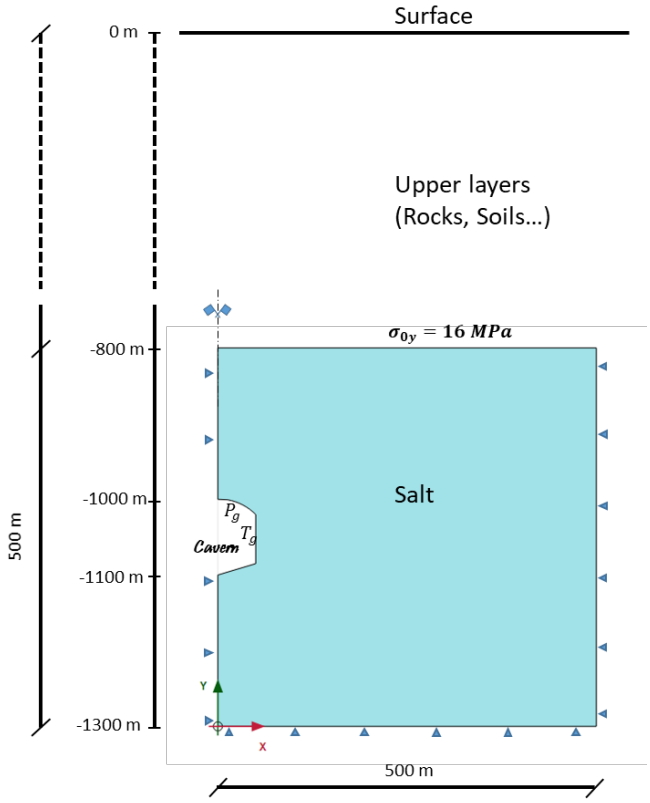

Figure 20. Deep Salt Cavern model geometry and boundary conditions

The cavern height is 100m and its diameter is 100m. It is located at the depth ranging from 1000m to 1100m in an *Asse salt formation* (Figure 20). Due to the symmetry of the model and the cavern geometry, an axisymmetric model of 500 mx 500m is used in PLAXIS 2D (corresponding to a depth from 800 to 1300m), which is large enough compared to the cavern geometry so as to avoid boundary effects. Instead of modelling complex behaviour of gas stored in the cavern, we apply directly a gas temperature and a gas pressure conditions on the cavern wall as simplified boundary conditions. In the PLAXIS 2D model, the cavern is located between y=200m to 300m. The left boundary (symmetry axis), the base and the right far field boundary are fixed mechanically and closed for heat flow. The life cycle of the cavern includes (Serbin, et al., 2015):

- Excavation by salt leaching
- Gas injection at high temperature and high pressure (Pressurisation)
- Storing of gas at maximum pressure
- Gas withdrawing for energy use (Depressurisation)
- Idling phase: storing of gas at minimum pressure

Except for excavation, the other phases are repeated seasonally.

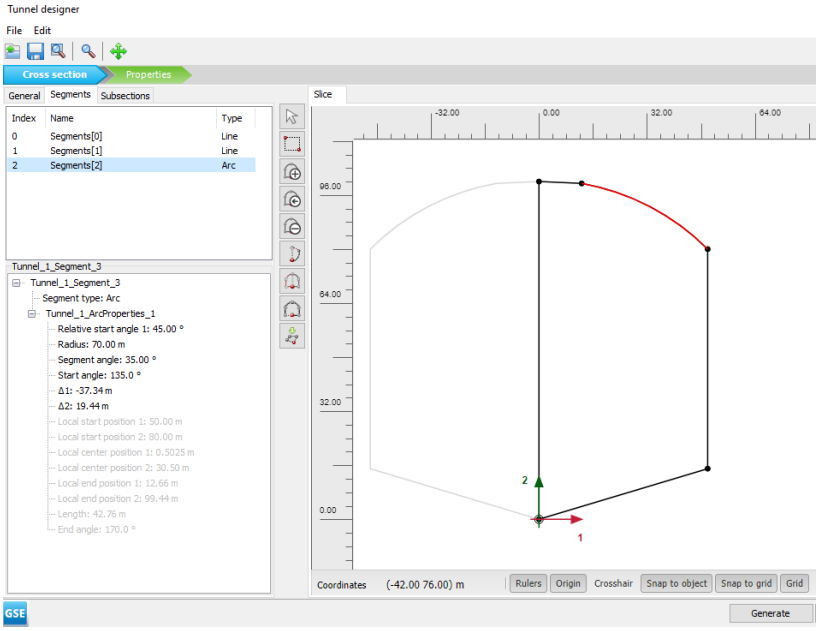

Figure 21. Tunnel designer tool to create the cavern geometry

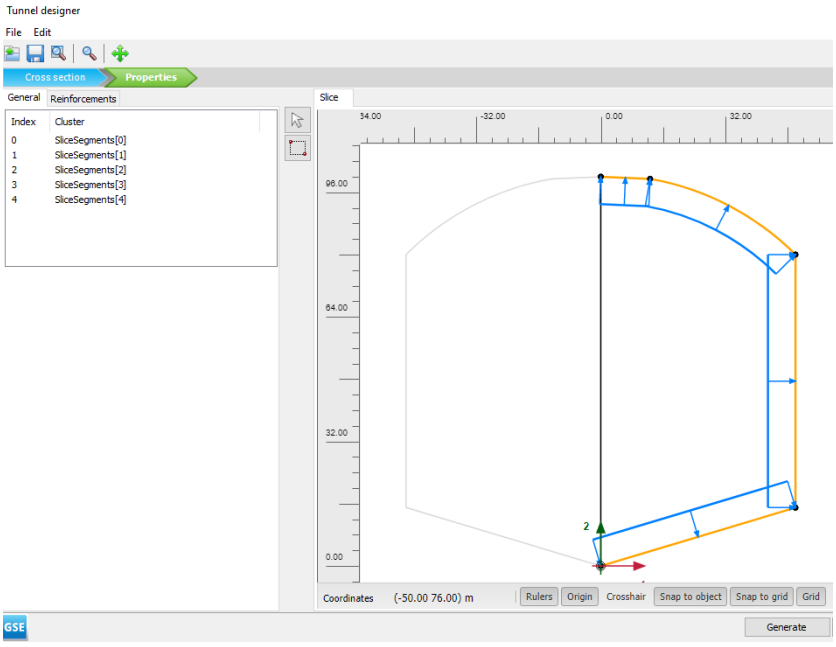

Figure 22. Creating boundary conditions at the cavern wall

To generate the shape of the cavern, the tunnel designer tool with 3 sections are used:

- Line 1: (0,0) to (50,15)
- Line 2: (50,15) to (50,80)
- Arc: start angle 45°, radius 70m, segment angle 35°

2 subsections are also used to get a closed geometry of the cavern as in Figure 21.

At the cavern wall, a *temperature boundary condition* and a normal *force perpendicular to the wall* are set in the tunnel properties as in Figure 22.

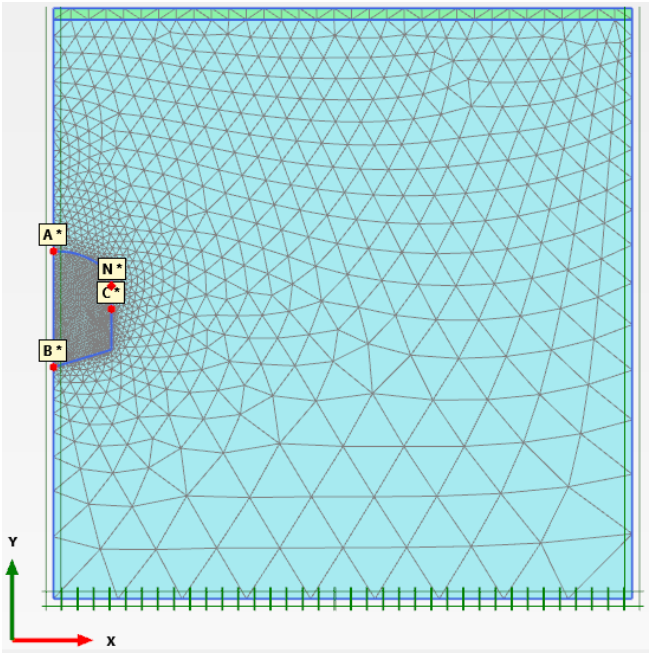

Figure 23. Model mesh and boundary conditions

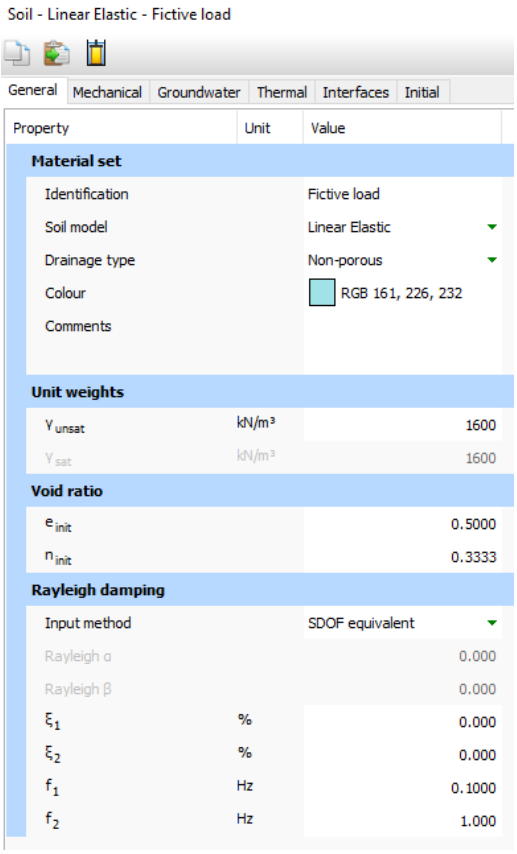

Figure 24. Fictive load layer geometry and properties

A general fine mesh is used due to complex phenomena involved. However, the mesh is refined around the cavern wall and coarsened at far field by setting a maximum coarseness factor of 8 (see Figure 23). Moreover, the effect of all the upper layers can be simulated by a line load or by using a fictive material layer which represent an equivalent weight. In this example, we use a 1m thick layer (see Figure 23) composed of a fictive non-porous very stiff material with a density of 1600 kN/m^2 (see Figure 24) to generate a vertical stress boundary condition of 16 MPa at the upper boundary of the model (Figure 20).

In Figure 23, some points are selected for later analyses, including nodes A (0,300); B (0,200); C (50,250.2); and stress point N (50.08, 270.3).

Parameters	Asse Rock Salt
Shear modulus G	8.846 GPa
Poisson's ratio ν	0.3
Density	20.4kN/m3

Void ratio	0.02
Specific heat capacity	858.6 10^3 J/t/°C
Thermal conductivity	5.4 W/m/K
Isotropic volumetricthermal expansion	8.4 10^{-5} 1/K
1st Creep exponent N_1	2.7
1st Creep parameter A_1	0.05 1/day
2nd Creep exponent N_2	6.8
2nd Creep parameter A_2	0.02
1st Temp.-related term $\frac{Q_1}{R}$	4800
2nd Temp.-related term $\frac{Q_2}{R}$	7800
Cohesion C	3000 KPa
Friction angle Phi	15^0
Dilation angle Psi	5^0
Tensile strength sig_T	1000 KPa

Table 4. Parameters for verification examples

The material parameters of Asse Rock Salt are summarised in Table 4. The N2PC double power creep parameters of this rock salt are taken from the steady state creep fitting presented in (Gunther, et al., 2015). The other typical parameters of rock salt, including elastic, thermal and density are taken from (Bottcher, et al., 2017) (Zhu, et al., 2017). They are shown in Table 4 Figure 25 and Figure 26.

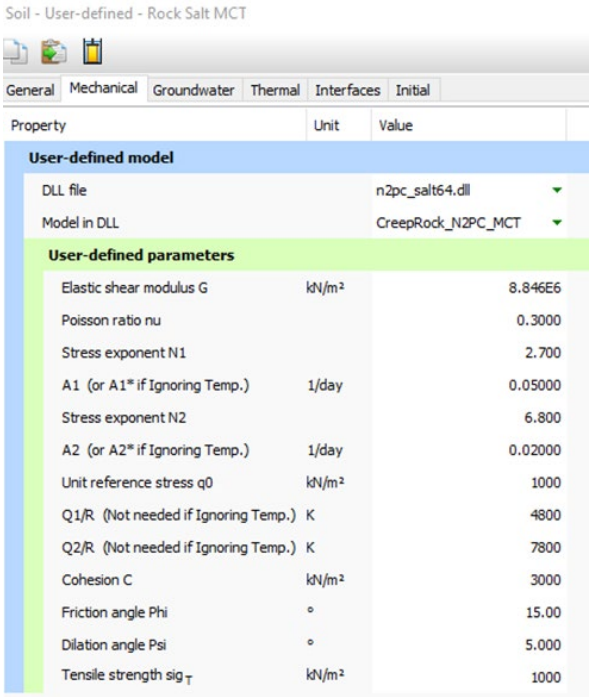

Figure 25. Asse Rock Salt constitutive parameters

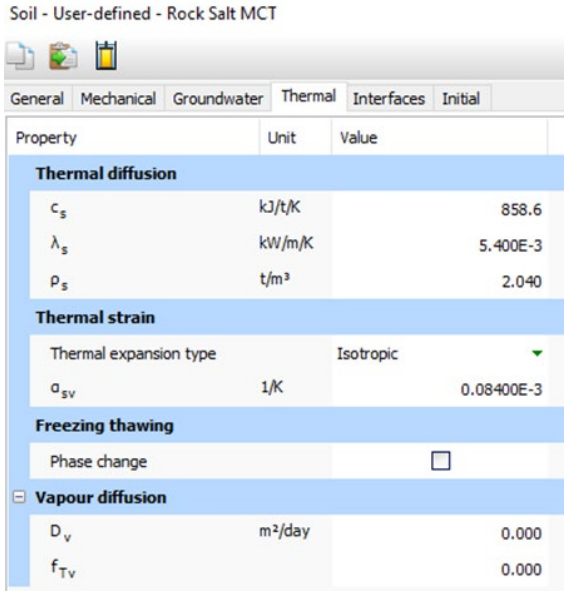

Figure 26. Asse Rock Salt thermal parameters

4.2 Model calculations

The 2 years simulation is carried out in the following phases. During each year, a cycle of pressurisation, storing, depressurisation, and idling is fully modelled. The input loading values are based on the realistic data from (Serbin, et al., 2015)

Initial Phase

During the initial phase, the initial stresses and temperatures are generated, using *K0 procedure* and *Earth gradient* modes.

In rock mechanics, the ratio between horizontal and vertical in situ stresses may depend on the considered depth. Following (Brown & Hoek, 1978) we take K_0=1.2, corresponding to the depth range (from 800 to 1300m) in the present study. This value is set in the *RockSalt material/Initial tabsheet*. The value K_0=1.2 means that the horizontal tectonic stress is higher than the vertical stress, which is often met in deep rock formation.

The average earth gradient in the upper formations is estimated 0.02 K/m, allowing to assume the temperature at the top of the model (y=500m) equal to 310K. Following (Bottcher, et al., 2017) a smaller gradient of 0.011 K/m is taken in the Salt layer.

Initial Operation state Phase

As aforementioned, the mining process is not modelled. Instead, the mechanical and thermal steady state after excavation are modelled using *Plastic* with *Steady-State thermal flow* modes. During this phase, a uniform temperature of 310K and a gas pressure of 8MPa is applied to the cavern wall during the storage of the gas.

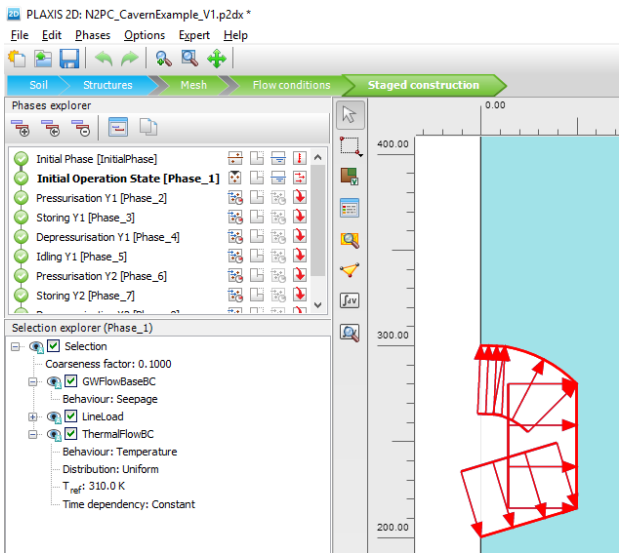

Figure 27. Initial Operation State Phase boundary conditions at the cavern wall

Pressurisation phase Y1 (1st year)

Starting from the initial state after excavation, gas is then injected intensively into the cavern during 20 days. This phase simulates the gas injection process. Pressurisation means that the pressure is increased from 8 MPa to 12 MPa and the temperature is also increased from 310 K to 325 K during 20 days, using a linear time dependent function *Heating 1* in PLAXIS 2D as shown in Figure 28. A transient calculation with Fully Coupled mode is therefore used.

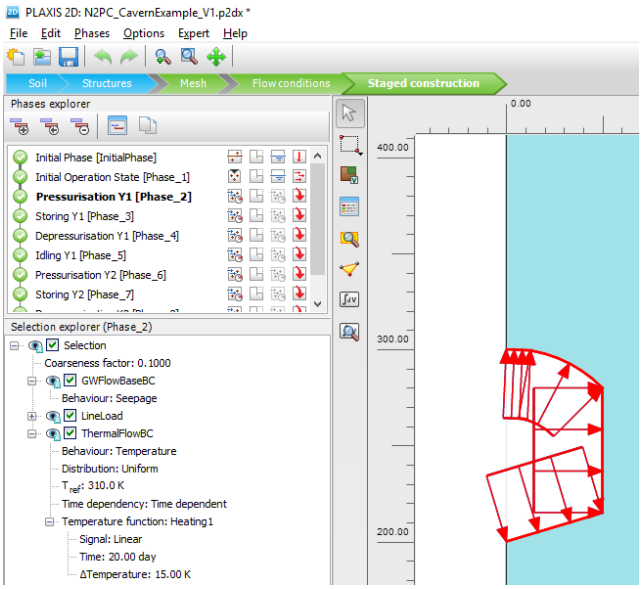

Figure 28. Gas pressurization phase

Storing Phase

After the gas injection, it is stored at the constant pressure and temperature during the remaining of the year (205 days). A fully coupled thermo-mechanical transient analysis is performed (see Figure 29).

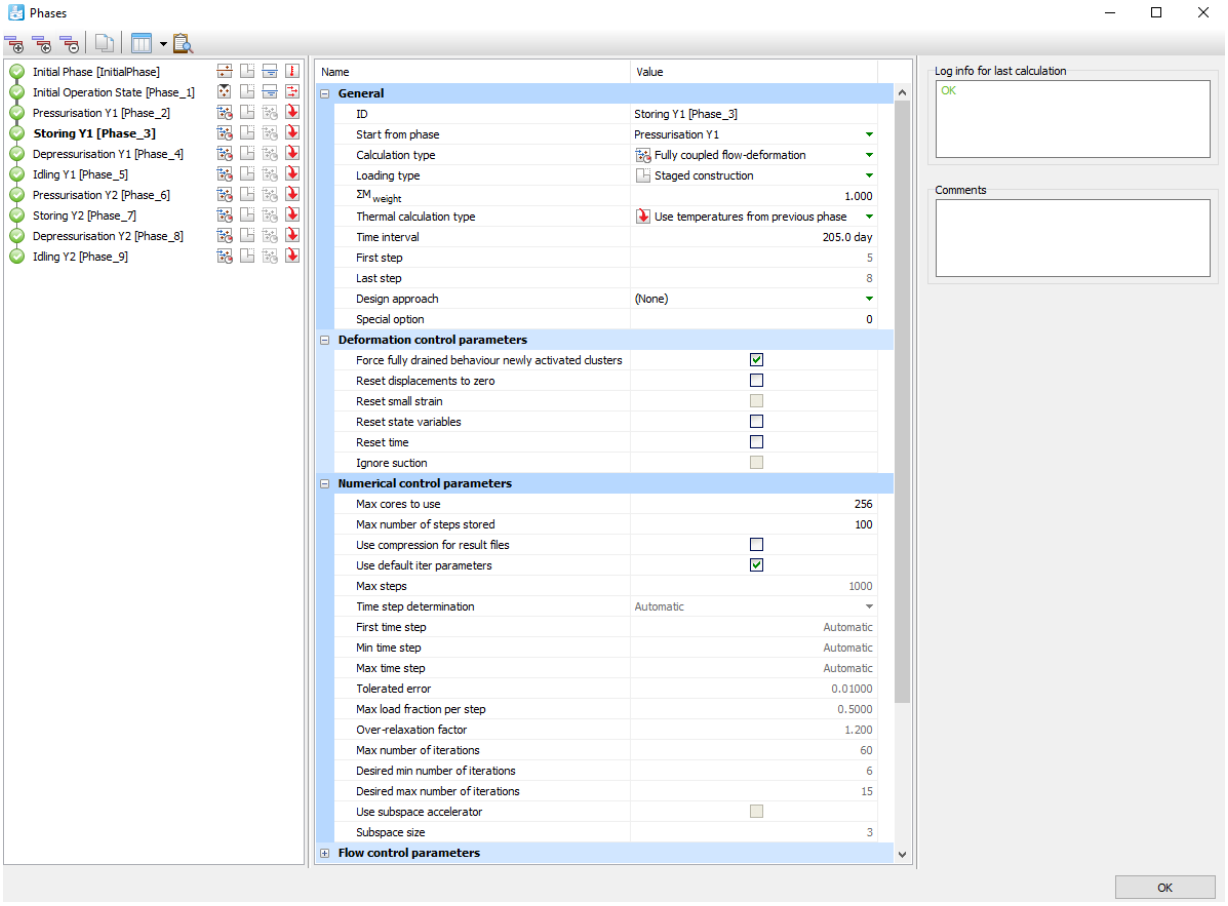

Figure 29. Storing phase Y1

Depressurisation Phase Y1

The gas is withdrawn during 20 days for energy production. The decrease of gas pressure also leads to a temperature decrease due to thermodynamic relationship of gas. A fully coupled thermo-mechanical transient analysis is performed (see Figure 29), where the temperature is reduced from 325 K to 295 K using a linear function Cooling, and the pressure is reduced to 5 MPa.

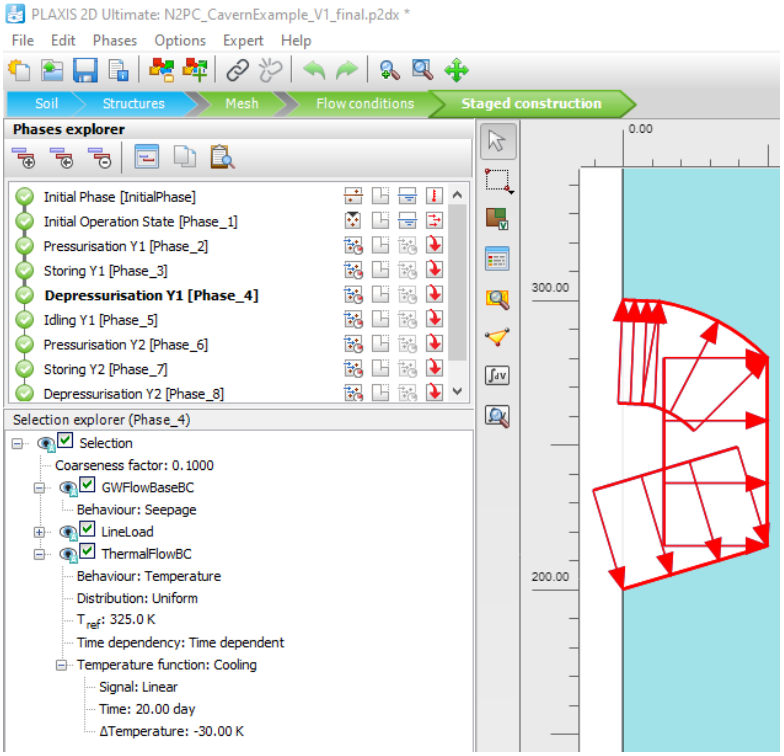

Figure 30. Depressurisation phase Y1 boundary conditions at the cavern wall

Idling Phase Y1

The gas is then stored at its minimum pressure of 5 MPa. The cavern is kept idle during the remaining of the year (120 days). A transient fully coupled analysis is therefore performed for this time interval.

This cycle is then repeated for year 2 (Phases denoted with Y2). The only difference is at the 2nd Pressurisation phase, where the temperature boundary conditions at the cavern wall is modelled by a linear function *Heating2* other than the temperature function *Heating1* used in Phase *Pressurisation Y1* (Figure 31). This is to model the temperature increase from 295 K (previous idling phase) to 325 K, i.e., interval of 30 K, instead of from 310 K (initial state) to 325 K as in the 1st Pressurisation phase.

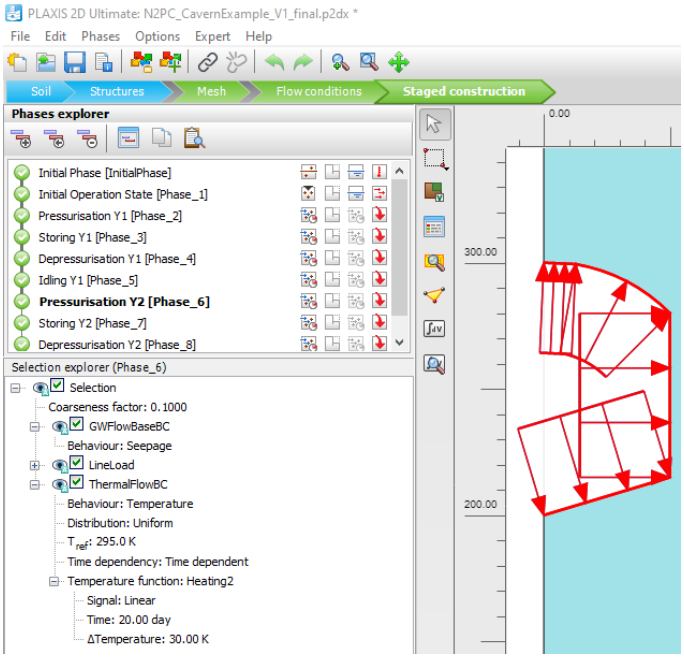

Figure 31. Temperature boundary condition for Pressurisation Y2 Phase

4.3 Numerical results

Assessing gas storages safety requires many factors. Among them, we present here 2 important analyses for cavern stability.

Convergence analysis

It is important to estimate the convergence, mainly the volume loss of the storage due to salt creep. Figure 32 shows the radial displacement at the right cavern wall (point C as indicated in Figure 23). It relates to the change of the cavern radius. It is seen that the cavern radius is getting smaller due to the creep effect. The convergence rate is highest during once the cavern is kept idle (Idling Phases Y1 and Y2). This is logical because the gas is kept at minimum pressure and the deviatoric stress is smallest during those phases.

Figure 33 show the vertical displacements at the roof and floor of the cavern. It is observed that the floor moves upward, while the roof moves downward, which points out the creep convergence effect. Again, the convergence rate is highest at Idling phases.

It is also noted that the creep convergence exhibits a transient behaviour although the constitutive model only takes the steady-state creep behaviour into account. This is consistent with the “geometrical transient creep” due to stress redistribution around the cavity as reported in previous works (Bérest, et al., 2017)

After 2 years, the cavern height lost 30cm and its radius lost around 15cm. Rough estimations lead to a loss of 0.9% of the cavern volume. The numerical results are at the same order of magnitude as reported in (Serbin, et al., 2015).

A small difference is also observed when comparing the displacements obtained with N2PC and N2PC-MCT. This is due to time-independent plastic deformation generated by the plastic mechanism incorporated in the N2PC-MCT model. The difference is however quite small, which suggests that in this case viscoplastic creep strains dominate over plastic strains. Therefore, if deformation is the primary focus of the analysis, N2PC model (without a failure mechanism) can provide satisfactory results

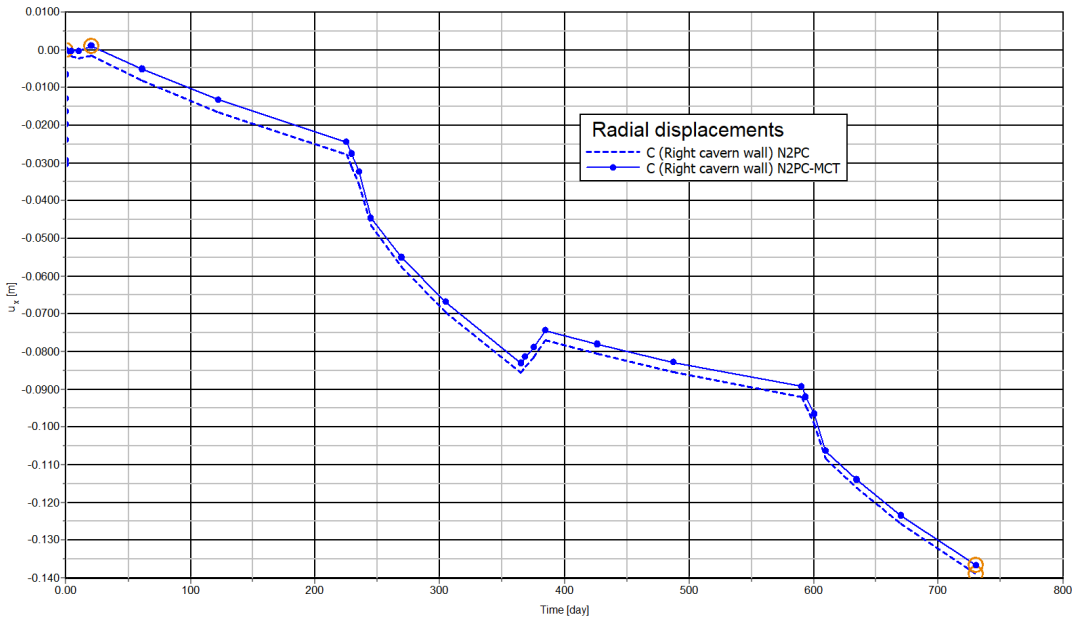

Figure 32. Time evolution of the radial displacement at the right side of the cavern (Point C)

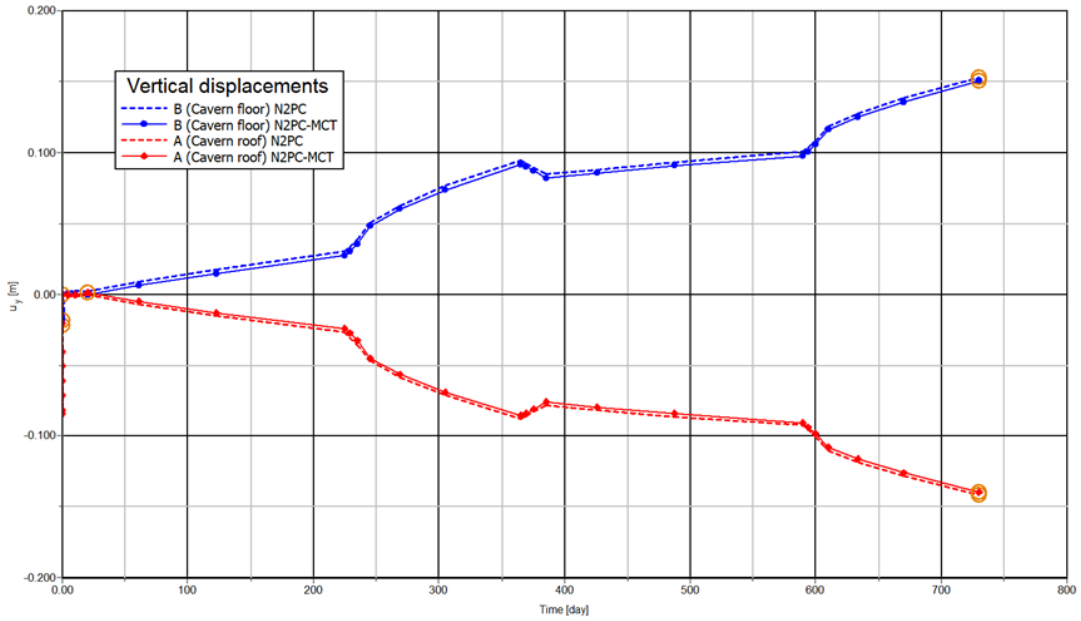

Figure 33. Time evolution of the vertical displacement at the roof and floor of the cavern (Point A and B)

Stress analysis

Apart from convergence problems, stresses, especially tensile stresses, are also a critical issue. This may lead to fracturing of the rock mass and thereby a permeability enhancement which induces gas leakage.

The radial (σ_{xx}), axial (σ_{yy}) and tangential (σ_{zz}) stresses at the point N (see Figure 23) at the vicinity of the cavern wall are plotted in Figure 34. It is observed that the axial stress follows the same stress path directly induced by boundary conditions at this wall. During pressurization, the tangential stress is increasing (less compressive). During depressurization, the tangential stress is however not decreasing. This may be explained by the cooling effect (see Figure 35) where a temperature drop results in a tensile stress near the cavern wall. Note that in Figure 35 the highest temperature is somewhere inside the rock mass but not at far field because the previous storing phase does not reach the steady state yet. During the creep phases (Idling or storing phases), the stress state tends to isotropic (equilibrium).

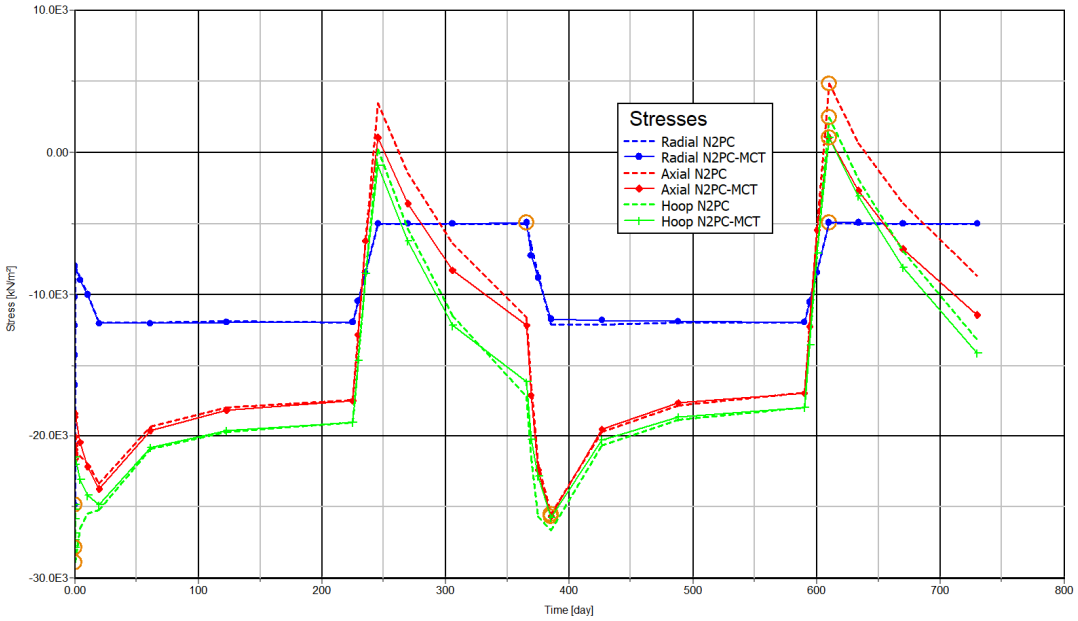

Figure 34. Stresses at point N at the vicinity of the cavern wall

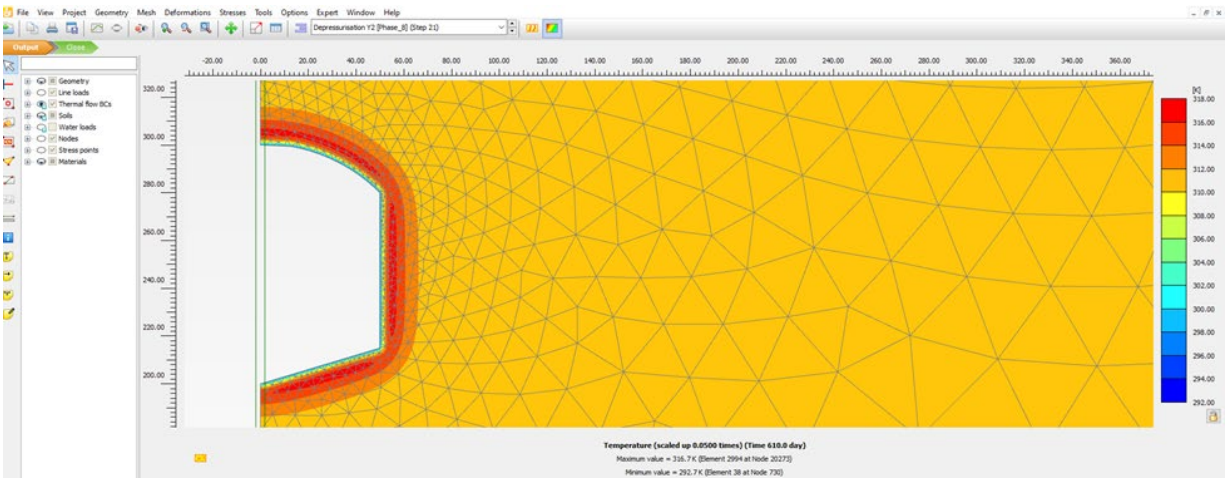

Figure 35. Temperature profile at the end of the 2nd Depressurisation Phase

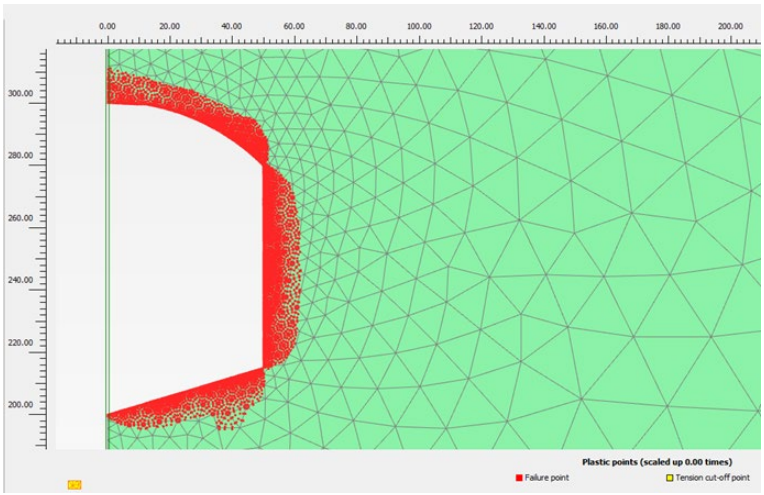

(a)

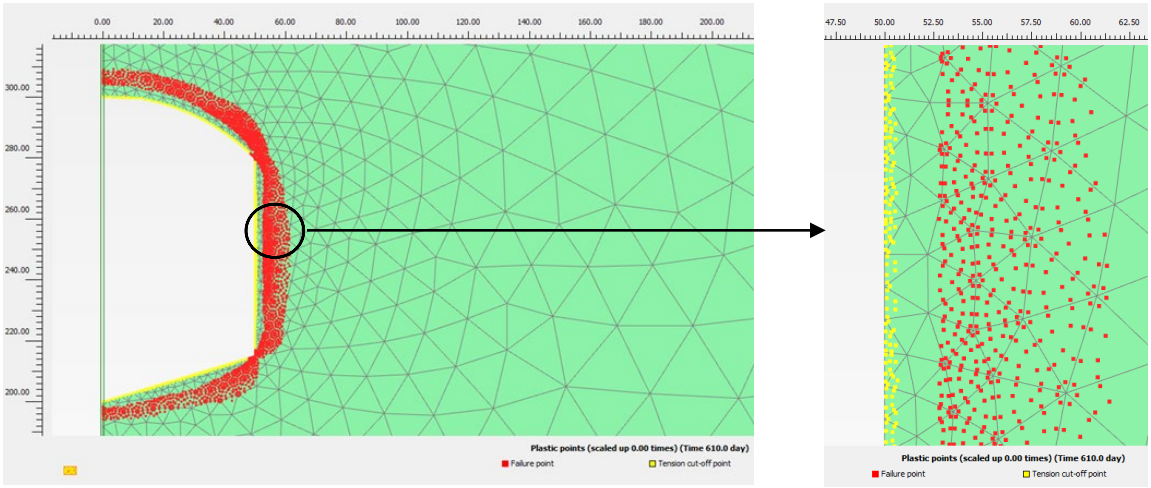

(b)

Figure 36: (a) Failure points at the end of Initial operation phase, (b) Failure points and tension cut off points at the end of Depressurization Y2 phase

The cooling effect seen in Figure 34 is widely reported in the literature (Berest, et al., 2012) (Bottcher, et al., 2017) (Berest, 2011) (Serbin, et al., 2015). At this stress point N, the tangential and axial stresses may be tensile and fracturing may develop. It is seen that by using N2PC-MCT model, theses stresses are cut-off at the tensile strength. To further investigate, the plastic points are shown in Fig 37. A tensile zone (with tensile failure points) appears at the vicinity of the cavern.

To highlight the cooling effect, the simulation is repeated but by setting the thermal expansion coefficient equal to zero. The stresses at point N are plotted again in Figure 36. It is readily seen that without thermal expansion the tensile stresses are not developed.

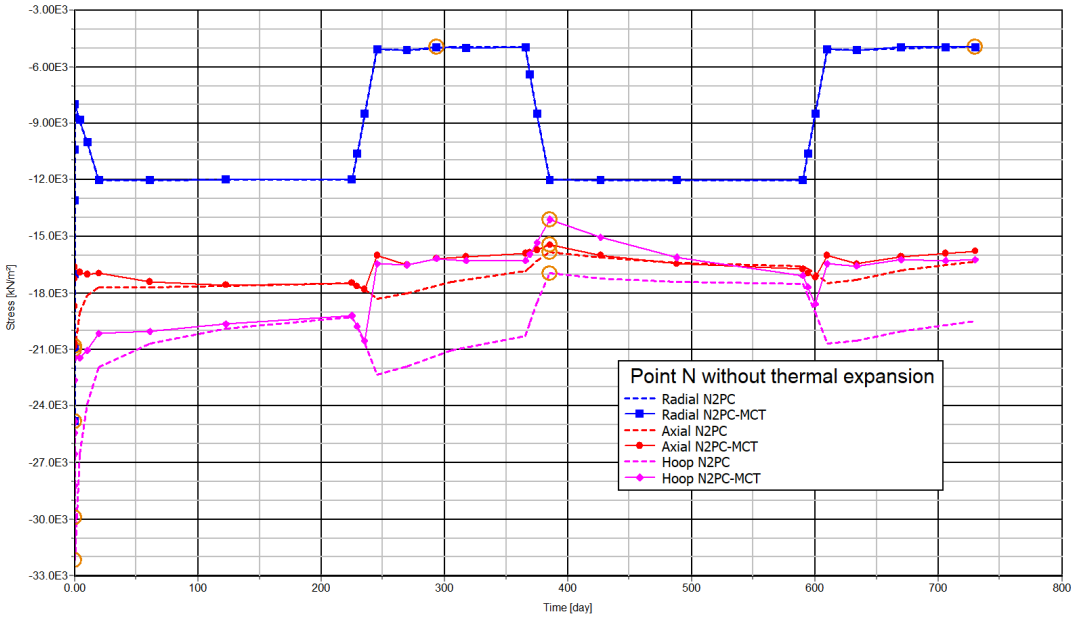

Figure 37. Stresses at point N at the vicinity of the cavern wall without thermal expansion

5 Conclusions

N2PC, a constitutive model for creep of rocks, especially rock salt, as well as its extended version N2PC-MCT, have been implemented in PLAXIS as UDSMs. These models are a generalised version of the classic Norton model with 2 power components. For N2PC-MCT, a Mohr-Coulomb with Tension cut-off plastic failure criterion is also included. A robust and efficient implementation with automatic local sub-stepping was performed to ensure both numerical accuracy, stability as well as user-friendliness. Both isothermal and non-isothermal versions are available so that the model can be used for both PLAXIS products, including SoilTest facility, PLAXIS 2D and PLAXIS 3D. The model implementation has been verified by comparing the numerical and analytical solutions for basic laboratory tests such as relaxation tests and constant strain rate tests. A practical example has been performed to illustrate the applicability of the model together with PLAXIS to the thermo-mechanical analysis of a gas storage in a deep salt formation. The N2PC model, with only 8 parameters, can provide satisfactory elements especially for deformation analysis, while the extended version N2PC-MCT can provide further insights for stress analysis.

6 References

Berest, P., 2011. Thermomechanical Aspects of high frequency cycling in salt storage caverns. *International Gas Union Research Conference.*

Berest, P., Ghoreychi, M., Hadj-Hassen, F. & M., T., 2012. *Mechanical Behaviour of Salt VII.* Paris: Taylor & Francis.

Bérest, P., Karimi-Jafari, M. & Brouard, B., 2017. Geometrical versus rheological transient creep closure in a salt cavern. *Comptes Rendus Mecanique,* Volume 345, p. 735–741.

Bottcher, N., Gorke, U., Kolditz, O. & Nagel, T., 2017. Thermo-mechanical investigation of salt caverns for short-term hydrogen storage. *Environmental Earth Science,* p. 76:98.

Brown, E. & Hoek, E., 1978. Trends in Relationships between Measured In-Situ Stresses and Depth. *Int. J. Rock Mech. Min. Sci. & Geomech. Abstr.,* Volume 15, pp. 211-215.

Bui, T. et al., 2017. A thermodynamically consistent model accounting for viscoplastic creep and anisotropic damage in unsaturated rocks. *International Journal of Solids and Structures,* Volume 117, pp. 26-38.

Cornet, J., Dabrowski, M. & Schmida, D., 2018. Long term creep closure of salt cavities. *International Journal of Rock Mechanics and Mining Sciences,* Volume 113, pp. 96-106.

Fokker, P., 1994. *The behaviour of Salt and Salt Caverns,* Delft: TU Delft .

Gramheden, R. & Hokmark, H., 2010. *Creep in jointed rock masses: State of knowledge,* Stockholm: SKB.

Gunther, R., Salzer, K., Popp, T. & Ludeling, C., 2015. Steady-State Creep of Rock Salt: Improved Approaches for Lab Determination and Modelling. *Rock Mech Rock Eng.*

Hudson, J., 1993. *Comprehensive Rock Engineering: Rock Testing and Site Characterization.* Oxford: Pergamon.

Mahnken, R. & Stein, E., 1989. Adaptive Time Step control in Creep Analysis. *International journal for numerical methods in Engineering,* Volume 28, pp. 1619-1633.

Norton, F. H., 1929. *Creep of Steel at High Temperatures,* New York: McGraw-Hill Book Company.

Plaxis, 2021. *PLAXIS 2D Material Model Manual,* s.l.: s.n.

Polyanin, A. & Zaitsev, V., 2017. *Handbook of Ordinary Differential Equations: Exact Solutions, Methods, and Problems.* s.l.:CRC Press/Chapman and Hall.

Serbin, K., Ślizowski, J., Urbańczyk, K. & Nagy, S., 2015. The influence of thermodynamic effects on gas storage cavern convergence. *International Journal of Rock Mechanics & Mining Sciences,* Volume 79, p. 166–171.

Simo, J. & Hughes, T., 1997. *Computational Inelasticity.* New York: s.n.

Zhu, C., Shen, X., Arson, C. & Pouya, A., 2017. Numerical study of thermo-mechanical effects on the viscous damage behavior of rock salt caverns. *ARMA 17-353.*